FACULTY OF TEXTILE ENGINEERING TUL

NEW SYSTEM OF ELECTRODES FOR SUPERCAPACITOR

Qingyan Peng, M.Eng.

SUMMARY OF THE THESIS

Title of the dissertation:	**New system of electrodes for supercapacitor**
Author:	**Qingyan Peng, M.Eng.**
Doctoral Program:	**Textile Engineering**
Form of study:	**Full time**
Training department:	**Department of Material Engineering**
Supervisor:	**Mohanapriya Venkataraman, M.Tech., M.F.Tech., Ph.D.**
Consultant:	**prof. Ing. Jiří Militký, CSc.**

Composition of the dissertation defence committee:

Chairman:	
doc. Ing. Jiří Chvojka, Ph.D.	FT TUL, Department of Nonwovens and Nanofibrous Materials
Vice-charmain:	
prof. Ing. Luboš Hes, DrSc., dr.h.c.	FT TUL, Department of Textile Evaluation
doc. Ing. Michal Petrů, Ph.D.	FS TUL, Department of the Design of Machine Elements and Mechanisms
doc. Ing. Veronika Tunáková, Ph.D.	FT TUL, Department of Material Engineering
Assoc. Prof. Guocheng Zhu (opponent)	College of Textile Science and Engineering, Zhejiang Sci-Tech University
Ing. Karel Kupka, PhD.	TriloByte Statistical Software, s.r.o.
Ing. Josef Večerník CSc.	Večerník, s.r.o.

An opponent who is not a member of the commission:

Prof. Henry, Yi Li	Department of Materials, School of Natural Sciences, The University of Manchester

The dissertation can be consulted at the Department of Doctoral Studies, Faculty of Textiles, Technical University of Liberec.

Liberec, 2024

Abstract

This study introduces a novel approach for developing flexible supercapacitors, which employs reactive inkjet printing (RIP) technology to deposit and in-situ reduce single/composite graphene inks on various fabric substrates. Utilizing advanced inkjet printing techniques, this method allows for precise material deposition and compositional tuning, enabling the fabrication of high-performance flexible electrodes suitable for supercapacitors. The first part of this study focuses on creating ultralight pure reduced graphene oxide (rGO) all-solid-state supercapacitors using polyvinylidene difluoride (PVDF) electrospun nanofiber substrates. The rGO/PVDF electrodes are fabricated at various layer thicknesses by inkjet printing and optimized through in-situ chemical reduction using L-ascorbic acid (AA). The impact of the rGO print layers on their electrochemical properties and other performance metrics is analyzed using the Interface 1010E™ potentiostat and its accompanying setup.

Additionally, advanced analytical techniques such as SEM, EDX, and XPS are employed to assess changes in the morphology and chemical structure of the electrode surfaces. This part of the study demonstrates that GO ink uniformly covers the surface of the PVDF nanofibers and is successfully reduced in-situ to rGO. The rGO layers achieve high conductivity and good electrochemical performance on the nanofiber membrane substrates, exhibiting a maximum specific capacitance of 85.66 F/g. Furthermore, the rGO/PVDF electrodes show strong cycle stability, maintaining 93% efficiency after 4000 charge-discharge cycles at a current density of 2 A/g.

Based on the work of the first part, the second part of the study involves fabricating composite flexible supercapacitors by combining Ag nanoparticles (AgNPs) with rGO via RIP technology onto flexible polypropylene (PP) nonwoven fabrics. This combination aims to utilize the high electrical conductivity of Ag and the capacitive properties of rGO to significantly improve the overall electrochemical characteristics of the composite electrodes. The Ag/rGO/PP electrodes are fabricated using a customized inkjet printing process that includes an additional print head for depositing silver nitrate ($AgNO_3$) ink, which is simultaneously printed with GO ink and AA reducing agent, followed by in-situ and synchronous reduction. In this process, Ag nanoparticles are directly formed between rGO sheets, physically preventing rGO aggregation, thereby enhancing the charge transfer rate and boosting the capacitive performance of the electrodes. Conductivity tests show that the introduction of Ag nanoparticles significantly reduces the surface resistance of the electrodes. Electrochemical tests reveal that the Ag/rGO composite electrodes exhibit a high specific capacitance of up to 800.30 F/g and an energy density of 70.9 Wh/kg at a current density of 0.25 mA/cm², along with excellent charge-discharge stability.

Keywords: Reactive inkjet printing; Supercapacitors; Flexible; Reduced graphene oxide; Silver

Abstrakt

Tato práce představuje nový přístup k vývoji flexibilních superkondenzátorů, které využívají technologii reaktivního inkoustového tisku (RIP) k nanášení a in-situ“ redukci jednoduchých/kompozitních grafénových inkoustů na různé textilní substráty. Tato metoda využívá pokročilé techniky inkoustového tisku a umožňuje přesné nanášení materiálu a ladění složení, což umožňuje výrobu vysoce výkonných flexibilních elektrod vhodných pro superkondenzátory. První část této studie se zaměřuje na vytvoření ultralehkých čistých pevných superkondenzátorů s redukovaným oxidem grafénu (rGO) při použití nanovlákenných substrátů z polyvinylidenfluoridu (PVDF). Elektrody rGO/PVDF byly připraveny v různých tloušťkách vrstev inkoustovým tiskem a optimalizovány chemickou redukcí in-situ pomocí kyseliny L-askorbové (AA). Dopad tiskových vrstev rGO na jejich elektrochemické vlastnosti a další výkonnostní metriky byl analyzován pomocí potenciostatu Interface 1010E™ a jeho příslušenství. Kromě toho se k posouzení změn v morfologii a chemické struktuře povrchů elektrod použily pokročilé analytické techniky, jako je SEM, EDX, a XPS. Bylo ukázáno, že GO inkoust rovnoměrně pokrývá povrch PVDF nenavlášen a je úspěšně redukován in-situ na rGO. Vrstvy rGO dosahují vysoké vodivosti a dobrého elektrochemického výkonu na nanovlákenných membránových substrátech, přičemž vykazují maximální specifickou kapacitu 85,66 F/g. Kromě toho elektrody rGO/PVDF vykazují silnou stabilitu cyklu, udržují 93 % účinnost po 4000 cyklech nabití a vybití při proudové hustotě 2 A/g. Na základě výsledků z první části, byla druhá část studie zaměřena na přípravu kompozitních flexibilních superkondenzátorů kombinováním Ag nanočástic (AgNP) s rGO pomocí RIP technologie na flexibilní polypropylenové (PP) netkané textilii. Tato kombinace měla za cíl využít vysokou elektrickou vodivost Ag a kapacitní vlastnosti rGO k výraznému zlepšení celkových elektrochemických charakteristik kompozitních elektrod. Elektrody Ag/rGO/PP byly připraveny pomocí modifikovaného procesu inkoustového tisku, který zahrnuje další tiskovou hlavu pro nanášení inkoustu s dusičnanem stříbrným ($AgNO_3$), který je současně potištěn inkoustem obsahujícím GO a redukční činidlo AA. Následovala „in-situ“ redukce. V tomto procesu se Ag nanočástice přímo tvoří mezi plátky rGO, což fyzicky zabraňuje agregaci rGO, čímž se zvyšuje rychlost přenosu náboje a zvyšuje se kapacitní výkon elektrod. Testy vodivosti ukázaly, že zavedení Ag nanočástic výrazně snižuje povrchový odpor elektrod. Elektrochemické testy prokázaly, že kompozitní elektrody Ag/rGO vykazují vysokou specifickou kapacitu až 800,30 F/g a hustotu energie 70,9 Wh/kg při proudové hustotě 0,25 mA/cm², spolu s vynikající stabilitou nabíjení a vybíjení.

Klíčová slova: Reaktivního inkoustový tisk; Superkondenzátory; Flexibilní materiál; Redukovaný oxid grafénu; stříbro

摘要

本研究介绍了一种开发柔性超级电容器的新方法，该方法采用反应喷墨打印（RIP）技术将单一/复合石墨烯墨水沉积并原位还原到各种织物基材上。利用先进的喷墨打印技术，该方法可以精确沉积材料并调节组成，使得制造适用于超级电容器的高性能柔性电极成为可能。本研究的第一部分重点在于使用聚偏二氟乙烯（PVDF）静电纺纳米纤维基材创建超轻的纯还原氧化石墨烯（rGO）全固态超级电容器。通过喷墨打印在不同层厚下制造 rGO/PVDF 电极，并通过使用 L-抗坏血酸（AA）进行原位化学还原来优化这些电极。使用 Interface 1010E™ 电位仪及其配套设置分析 rGO 打印层对其电化学性能和其他性能指标的影响。 此外，采用 SEM、EDX 和 XPS 等先进分析技术评估电极表面形貌和化学结构的变化。研究表明，GO 墨水均匀覆盖 PVDF 纳米纤维表面，并在原位成功还原为 rGO。rGO 层在纳米纤维膜基材上表现出高导电性和良好的电化学性能，表现出 85.66 F/g 的最大比电容。此外，rGO/PVDF 电极显示出强的循环稳定性，在 2 A/g 的电流密度下经过 4000 次充放电循环后保持 93%的效率。 基于第一部分的工作，研究的第二部分涉及通过 RIP 技术将 Ag 纳米颗粒（AgNPs）与 rGO 结合在柔性聚丙烯（PP）无纺布上制造复合柔性超级电容器。这种组合旨在利用 Ag 的高电导率和 rGO 的电容特性显著改善复合电极的整体电化学特性。Ag/rGO/PP 电极采用定制的喷墨打印工艺制造，其中包括一个用于沉积硝酸银（AgNO3）墨水的附加打印头，该打印头与 GO 墨水和 AA 还原剂同时打印，然后进行原位和同步还原。在此过程中，Ag 纳米颗粒直接形成于 rGO 片之间，物理上防止 rGO 聚集，从而增强电荷传递速率并提高电极的电容性能。导电性测试表明，引入 Ag 纳米颗粒显著降低了电极的表面电阻。电化学测试显示，Ag/rGO 复合电极在 0.25 mA/cm²的电流密度下具有高达 800.30 F/g 的比电容和 70.9 Wh/kg 的能量密度，并具有优异的充放电稳定性。

关键词：反应喷墨打印；超级电容器；柔性；还原氧化石墨烯；银

Table of contents

1 Introduction

As society progresses, the burgeoning energy demand calls for advancements in energy storage solutions that are not only efficient but also adaptable to a range of applications. Typical devices for storing energy include lead-acid batteries, lithium-ion batteries, nickel-metal hydride batteries, and supercapacitors. Among a range of advanced energy retention systems, supercapacitors, with an emphasis on flexible versions, are distinguished by their rapid charge-discharge rate, wide operating temperature range, long lifespan, high power density, and high electrochemical stability under mechanical deformation [1, 2]. Supercapacitors are categorized into three types: electrochemical double-layer capacitors (EDLC), pseudo-capacitors, and hybrid supercapacitors.

The fabrication techniques for graphene-based supercapacitors are as varied as they are innovative. Electrodeposition and electroless deposition are widely used for coating surfaces with a thin layer of graphene. Chemical vapor deposition (CVD) allows for the growth of high-quality graphene films, while direct laser writing (DLW) offers a more controlled and patterned deposition of graphene, useful for designing micro-supercapacitors and flexible energy storage devices. Nonetheless, each of these techniques has its own limitations. Inkjet printing technology is a groundbreaking method that has transformed material production, especially in crafting and deploying advanced materials like GO [3]. This method operates by accurately depositing reactive ink droplets onto a base, facilitating the formation of a high degree of control over film uniformity, surface coverage, and thickness. Furthermore, the reactive nature of the ink allows for in-situ chemical reactions or post-deposition processing, which can be used to modify or enhance the properties of the printed material [4, 5]. Additionally, its adaptability to a broad array of substrate materials, including textiles, paper, polymers, metals, and ceramics, expands its practical applications [6-8].

Given the scarcity of reports on using inkjet printing technology to develop graphene supercapacitors, this study intends to investigate the potential and adaptability of this method. We seek to contribute to the emerging field by evaluating the practicality and performance of supercapacitors produced via inkjet printing, trying to broaden their potential application in modern energy storage systems.

2 Purpose and the aim of the thesis

The aim of this research is to develop and validate innovative electrode systems for supercapacitors that combine novel material science approaches with advanced manufacturing techniques to enhance performance characteristics, including energy density, flexibility, and durability. This project focuses on harnessing the electrochemical and electrical properties of rGO and silver nanoparticles (AgNPs) through inkjet printing technology to create flexible supercapacitors for energy storage applications.

The specific purposes are as follows:

- Synthesize and optimize the formulation of inkjet-printable rGO and AgNPs to ensure effective deposition and high-quality film formation.
- Utilize inkjet printing technology to fabricate flexible electrodes with uniform rGO and AgNPs layers, aiming for optimal consistency and functional integrity across various substrates.
- To set up an appropriate electrochemical testing system, including electrolyte selection (acidic electrolytes, alkaline electrolytes, neutral electrolytes), cell configuration (i.e., two-electrode or three-electrode setup), and testing range.

- Thoroughly assess the electrochemical performance, energy density, and durability of the fabricated supercapacitors under diverse operational conditions.
- Examination of changes in the chemical structure of electrode materials using techniques such as EDX, XPS, etc.

3 Overview of the current state of the problem

In accordance with the latest technological developments in electric devices regarding their cycle durability, charging speed, and particular power capabilities, supercapacitors are emerging as favourable options across various sectors needing significant energy throughput (such as hybrid electric vehicles) and consistent energy delivery (including precise automation systems, computer processors, and mobile electronic gadgets). Supercapacitors have attracted considerable interest due to their high specific capacitance, long life cycle, substantial power density, minimal maintenance requirements, lack of memory effect, safety features, and their role in bridging the gap between the high power density of capacitors and the large energy storage capacity of Graphene, characterized by its one-atom-thick two-dimensional structure, has gained prominence as a distinctive carbon-based material for energy storage applications. It is acclaimed for its outstanding electrical conductivity, chemical robustness, and extensive surface area. Its adoption in supercapacitors is advocated due to its high capacity for energy storage, which is independent of solid-state pore distribution, a stark contrast to other carbon derivatives like activated carbon or carbon nanotubes [9].

It is touted that graphene when fully utilizing its specific surface area, can achieve capacitance levels as high as 550 F/g [10]. The fabrication techniques for graphene-based supercapacitors are as varied as they are innovative. Electrodeposition and electroless deposition are widely used for coating surfaces with a thin layer of graphene. Chemical vapor deposition (CVD) allows for the growth of high-quality graphene films, while direct laser writing (DLW) offers a more controlled and patterned deposition of graphene, useful for designing micro-supercapacitors and flexible energy storage devices. Nonetheless, each of these techniques has its own limitations. Electrodeposition and electroless deposition can sometimes result in non-uniform coatings and may require complex setups [11]. CVD offers high-quality graphene films but requires a high-temperature environment, specific atmosphere, and special substrate for growth, which makes it energy-intensive [12]. Due to the concentrated energy required to induce material changes, DLW has specific substrate requirements. It is generally suited for substrates that can withstand high temperatures and possess surfaces conducive to laser interaction [13]. Inkjet printing technology is a groundbreaking method that has transformed material production, especially in crafting and deploying advanced materials like GO [3]. This method operates by accurately depositing reactive ink droplets onto a base, facilitating the formation of a high degree of control over film uniformity, surface coverage, and thickness. Furthermore, the reactive nature of the ink allows for in-situ chemical reactions or post-deposition processing, which can be used to modify or enhance the properties of the printed material [4, 5]. Additionally, its adaptability to a broad array of substrate materials, including textiles, paper, polymers, metals, and ceramics, expands its practical applications [6-8].

In conclusion, the current state of research on graphene-based supercapacitors highlights both the significant potential and the existing challenges. The exceptional properties of graphene and its derivatives offer a pathway to advanced energy storage solutions. However, achieving the optimal balance between material properties, fabrication techniques, and practical application remains a key area of focus for ongoing research. This report, due to the use of reactive inkjet printing (RIP) to combine rGO with AgNPs has shown promise in producing flexible, high-

performance electrodes. This method allows precise control over material deposition and composition, leading to enhanced electrochemical properties.

4 Used methods, study material

4.1 Materials

Steady, densely packed GO dispersion type I: water dispersion, 5 g/L, diameter 0.5-5 μm, was purchased from Graphene Supermarket® (USA), type II: water dispersion, 2 mg/mL, diameter 200-500 nm, was purchased from BioTools, Inc. (USA). Electrospun PVDF fibrous film (area density 6.74 g/m^2, thickness 70 μm) was acquired from CxI institute (Technical University of Liberec, Czech Republic), which exhibits excellent mechanical properties (Young's modulus of 15.6MPa, ultimate stress of 1.5MPa, and break strain of 66.0%). Polypropylene (PP) spun-bonded nonwoven fabric was obtained from the institute of textile architecture, Lodz University of Technology (area density 120g/m^2, thickness 0.52 mm). L-ascorbic acid (AA) silver nitrate ($AgNO_3$) pure pro analysis (p.a.) was purchased from Chempur (Poland). Poly (vinyl alcohol) (PVA) (Mw=72,000 g/mol), sulfuric acid (H_2SO_4) (95–97%), potassium chloride (KCl, powder, suitable for cell culture, BioReagent, ≥99.0%) were purchased from Poch (Poland). Glass microfiber filter membrane separator (GF/F Whatman™, USA, thickness 0.26 mm), isopropyl alcohol (⩾99.7%) pure pro analysis (p.a.) were obtained from Sigma-Aldrich Co. Appretan® N 9415, a commercial thermo-curable acrylate copolymer water-dispersible resin was purchased from Clariant International Ltd., Switzerland.

4.2 Sample preparation

4.2.1 Preparation of in-situ reduced rGO printed PVDF single electrode

A precursor current electrode was initially fabricated using a 250 Pfeiffer Vacuum system before applying the rGO-material electrodes. This process involved depositing a gold layer with a thickness of around 20 ~ 50 nm onto the electrospun PVDF substrate. The deposition was executed with a resistance vapor source regulated by current. Upon attaining a vacuum pressure of 0.0002 Pa, the gold was then deposited over a 5-minute period. Subsequently, a rectangular material electrode was constructed by depositing layers of rGO with a size of 10 mm × 10 mm, onto the existing current electrode's surface. The customized inkjet printing apparatus was utilized for applying rGO conductive layers onto electrospun PVDF membrane surfaces. This apparatus included nano-dispensing technology (ReaJet SK 1/080, Germany), control electronics, an ink pumping mechanism, dual ink tanks, a bi-directional (x-y) movement setup, and a computerized management system. For efficient printing, type I GO dispersion was filled into the first print head's ink tank, whereas the second was filled with AA solution. Drawing from our earlier optimization research, we determined that the ideal AA reduction concentration stands at 50 g/L[14]. A vector graphics editor crafted the print design, which was then converted into a line-art bitmap using raster image processing software. This bitmap, set at a resolution of 50 dpi, matching the x-y axis print head's positioning accuracy, was prepared for printing. The ejected droplet volume was approximately 10 nl. The procedure began by heating the hot plate to 120 °C and placing the electrospun PVDF film atop it. Following the 'sandwich' mode printing of the predetermined graphic by both print heads, the films remained on the hot plate for 15-20 minutes at the same temperature to ensure complete GO reduction. Afterward, the rGO-layered electrospun PVDF (rGO/PVDF) films were cleansed with deionized water for 15 minutes to eliminate any impurities or by-products that could adversely affect the electrochemical properties. The cleansing process was followed by drying the rGO/PVDF films in an oven at 60 ℃ for 30 minutes.

4.2.2 Assembling of in-situ reduced rGO printed PVDF all-solid-state supercapacitor

After that, the PVA-H_2SO_4 polymer electrolyte was synthesized through the following steps: Initially, 1g of H_2SO_4 was gradually introduced into 10 ml of distilled water. Sequentially, 1g of PVA was blended into the previously prepared H_2SO_4 solution at 80 ℃, accompanied by vigorous stirring until a clear solution was formed. For the construction of the all-solid-state supercapacitor, a GF/F Whatman^{TM} glass microfiber membrane separator was soaked in the PVA- H_2SO_4 polymer electrolyte. Finally, two rGO/PVDF freestanding electrodes were arranged in a sandwiched structure with the separator in between. The assembled all-solid-state rGO/PVDF supercapacitor was then compressed and left to dry under a force of 1MPa at ambient temperature for 12 hours.

4.2.3 Preparation of Ag ink for in-situ reduced Ag/rGO printed PP electrode

To explore how varying $AgNO_3$ concentrations affect the electrochemical properties of the supercapacitor, this work introduced a range from 0 mg/ml to 4 mg/ml, denoted as rGO, 0.0625Ag/rGO, 0.125Ag/rGO, 0.25Ag/rGO, 0.5Ag/rGO, 1Ag/rGO, 2Ag/rGO, and 4Ag/rGO, correspondingly. The specific preparation process involves fully dissolving varying gradient concentrations of $AgNO_3$ white powder into deionized water and storing the solution in a dark place for later use.

4.2.4 Fabrication of in-situ reduced Ag/rGO printed PP flexible supercapacitor

The fabrication process of the Ag/rGO conductive layer using a bespoke reactive inkjet printing (RIP) system. It is critical to ensure that the nonwoven fabric substrate is pre-treated to eliminate any spin finish, markings, or oily residues, which involves a comprehensive cleaning with isopropanol. Subsequently, to improve ink adherence and diminish surface irregularity, Appretan® N 9415 was uniformly applied onto the fabric via a pressure spray gun with a total of four layers. After each layer was applied, the PP would be transferred into an oven at 60°C for 20 minutes to cure the resin.

The initial step of creating the current electrode employed a standard 250 Pfeiffer Vacuum setup, preceding the addition of the Ag/rGO layer. This involved the precise deposition of a gold layer with a thickness ranging from 20 to 50 nm onto the PP nonwoven substrate by a controlled resistance evaporation source, executed over a duration of 5 minutes once a vacuum of 0.0002 Pa was achieved. The RIP system (ReaJet SK 1/080, Germany) was utilized to prepare the electrodes. The system employs three print heads, pre-filling the first and second print heads' ink chambers with type II GO dispersion and $AgNO_3$ solutions, respectively, while the third print head's chamber is filled with AA solution. This arrangement allows the two types of ink to be printed simultaneously onto the designated substrate, thereby simplifying the printing process. Drawing on prior optimization studies, the AA solution was set to a concentration of 50 g/L for effective reduction[14]. The printing process conducted on fabric was pre-heated to 120°C on a hotplate consists of depositing rGO and Ag in sequence. This method used a two-layer inkjet printing to ensure the desired conductive pattern is successfully formed. Each drop of ink has a volume of approximately 20-25 nL. Such a small volume ensures that reduction and solidification can be completed instantaneously and synchronously. Post-printing, to guarantee total reduction, the electrode undergoes an additional 15-minute heating period. Subsequent rinsing with deionized water and drying at 60°C for half an hour completes the process.

4.3 Measurement methods

4.3.1 Surface morphology testing

The structural features of the electrodes were analyzed using an Ultra-High Resolution Scanning Electron Microscope (UHR-SEM Zeiss Ultra Plus). Following this, the electrodes were subjected to energy dispersive x-ray (EDX) spectroscopy using an accelerating voltage of 10 kV. Given the natural conductivity of graphene, these measurements were performed without gold sputtering. Electron signal detection utilized both the InLens mode and the Angle-sensitive Backscatter (AsB) detector mode. The roughness of electrodes with the different number of printing layers was analyzed using a microscope (LEXT LS3000-IR) under a scanning area of 20 μm × 20 μm.

4.3.2 Electrical conductivity testing

The surface electrical resistance of the inkjet-printed electrodes was determined using a four-point probe method. Silver-plated brass cylindrical electrodes, each 2 mm in diameter, were arranged linearly at uniform intervals of 7 mm. A specified current was introduced through the outer probes, traversing the surface of the material and inducing a voltage drop across the two inner probes. This voltage drop was then measured while the current was maintained. The resulting voltage directly corresponds to the material's resistance between these probes. The surface resistance (Rs), expressed in ohms per square (Ω/sq), was subsequently calculated based on the formula (1) provided in reference [15].

$$\mathrm{Rs} = \frac{\pi \cdot U}{ln2 \cdot I} \qquad (1)$$

where U represents the voltage (V), and I represents the current (A).

4.3.3 X-ray photoelectron spectroscopy (XPS) testing

X-ray photoelectron spectroscopy (XPS) involves irradiating a sample with X-rays to excite the inner-shell electrons or valence electrons of the atoms or molecules into photoelectrons. The chemical composition of the sample surface, the binding energies of the elements, and their valence states are characterized by measuring the signals of these photoelectrons. The analyses were conducted using an M-probe system from Surface Science Instruments equipped with a monochromatic Al Kα radiation source (1486.6 eV). The experiments employed a beam spot measuring 200 μm by 750 μm to optimize the balance between spatial resolution and the examined area. A pass energy of 25 eV was used to achieve a spectral resolution of 0.74 eV. The energy scale was calibrated using the $4f_{7/2}$ peak of freshly deposited gold to ensure accuracy. An electron flood gun, set to 10 eV, was utilized to neutralize positive charge accumulation on insulating samples. Comprehensive XPS surveys revealed the atomic composition of the surfaces, and detailed high-resolution C 1s spectra were analyzed to delineate various carbon structures within the samples.

4.3.4 Electrochemical performance testing

An electrochemical workstation (**Fig. 1**) is an electronic instrument that controls the potential difference between a working electrode and a reference electrode. Both the working electrode and the reference electrode are components of the electrochemical cell. The electrochemical workstation controls the potential difference between these two electrodes by injecting current into a counter electrode. The electrochemical properties of the electrodes were evaluated using the Interface 1010E electrochemical workstation (Gamry Instruments, USA). Prior to attaching

samples, it is advised to conduct an initial open circuit test using cyclic voltammetry (CV) to ensure the workstation's stability and accuracy. This involves performing a voltammetric scan for 20 cycles ranging from 0V to the target operating voltage for each device. Key electrochemical tests such as electrochemical impedance spectroscopy (EIS), cyclic voltammetry (CV), galvanostatic charge/discharge (GCD), and assessments of electrochemical stability were carried out. EIS measurements were taken at the open circuit potential using a sinusoidal signal with an amplitude of 5 mV over a frequency range from 0.01 Hz to 100 kHz. Additionally, the specific capacity (Ah/g) was calculated from the CV curves using the formula (2) [16]:

$$\text{Specific capacity } (\text{Ahg}^{-1}) = \frac{\int i(V)dV(AV)}{m(g)\times v(Vs^{-1})\times 3600} \qquad (2)$$

where calculating the total voltammetric charge in ampere volts (AV) involves integrating the current across the voltage window; v represents the scan rate (V/s), and m denotes the mass of active materials loaded on the electrode (g). CV is typically performed at a low scan rate for battery materials to achieve optimal capacity readings. The specific capacity of the electrode can then be transformed into specific capacitance (F/g) using the formula (3) [16]:

$$\text{Specific capacitance } (\text{F/g}) = \frac{\text{Specific capacity } (Ah/g)\times 3600}{\Delta\text{V}(V)} \qquad (3)$$

where ΔV represents the voltage range of the individual electrode configuration (V). These calculations are essential for constructing a complete device with a capacitive negative electrode. Additionally, the specific capacitance (F/g) can be determined from the GCD curves using the formula (4) [17]:

$$\text{Specific capacitance } (\text{Fg}^{-1}) = \frac{2I_m \int \text{V}dt}{\Delta\text{V}^2} \qquad (4)$$

The current density of the electrode is denoted as $I_m = I/m$ (A/g), the integral of the current over time, expressed as $\int$Vdt quantifies the total charge passed, while ΔV refers to the operative voltage range (V). And the energy densities $(E_D, Wh/kg)$ and power densities $(P_D, W/kg)$ were derived from the experimental data using the equations (5) , (6) [17]. reference

$$E_D = \frac{1}{2} C_S \cdot V_0^2 \cdot \frac{1}{3.6} \qquad (5)$$

$$P_D = \frac{E\times 3600}{t} \qquad (6)$$

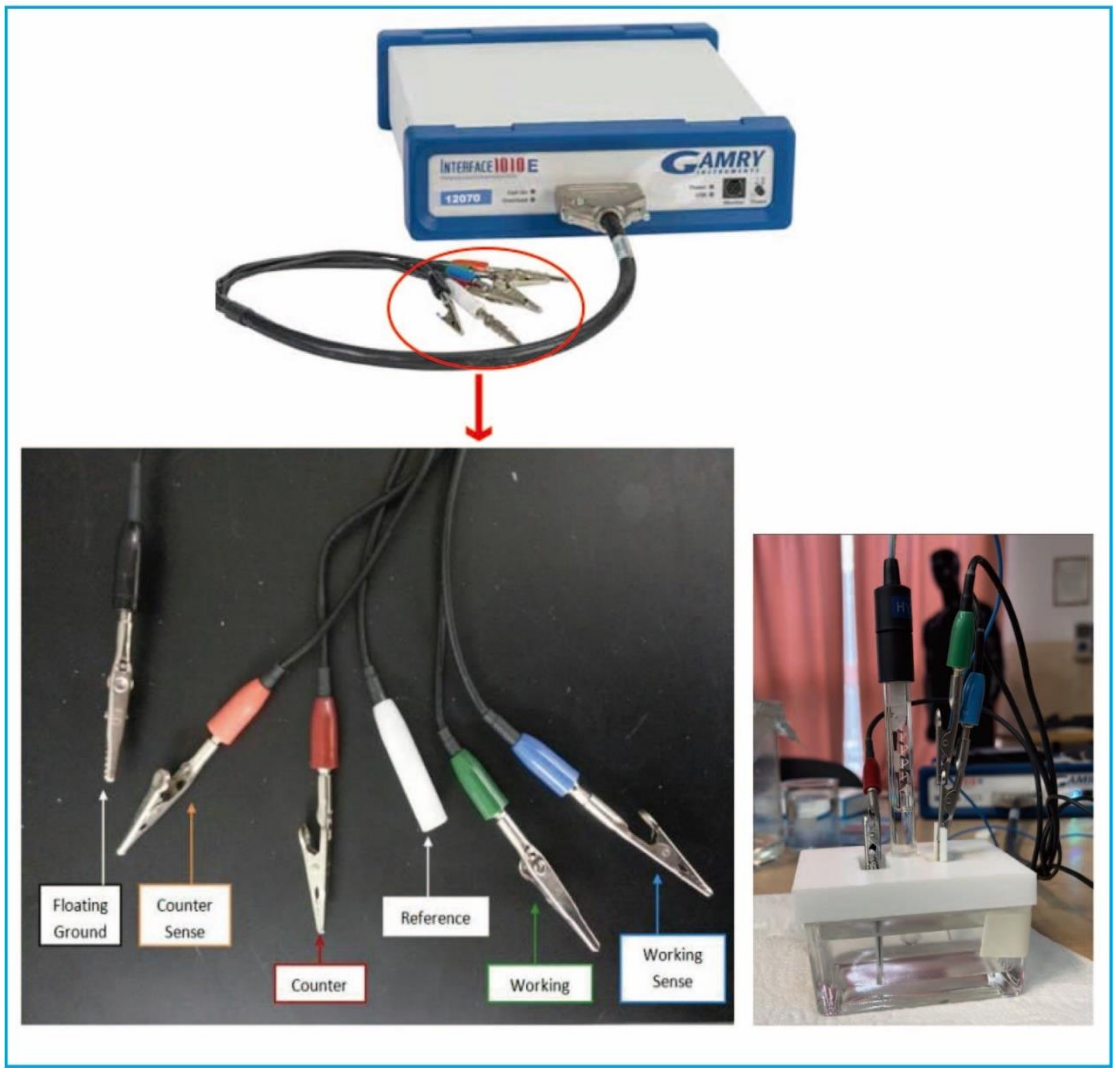

Figure 1. Image of the Interface 1010E™ potentiostat and various leads for electrochemical testing, including floating ground, counter sense, counter, reference, working, and working sense.

5 Summary of the results achieved

5.1 In-situ reduced rGO printed PVDF all-solid-state supercapacitor

5.1.1 SEM and confocal characterization of rGO-printed PVDF films

Fig. 2a presents an SEM image of the unmodified PVDF membrane. The image clearly shows that the PVDF nanofibers are uniform, bead-free, and have a smooth surface. The original PVDF displays a significant number of voids between the fibers, contributing to a surface roughness of Ra=3.57 μm, as depicted in **Fig. 2a-i**. It can be seen from **Fig. 2b** that after printing with rGO ink, numerous 'ridges' appear on the surface of the rGO pattern. These 'ridges' are a specific manifestation of the coffee ring effect, primarily due to solute concentration changes caused by solvent evaporation. During the in-situ reduction process, this effect is notably rapid as solvents evaporate, causing solutes or particles to accumulate at the droplet edges, thus forming ridge-like structures [5]. With each additional layer of printing, both the number and density of these ridges increase, thereby enhancing the surface roughness of the electrode. The roughness value Ra increases from 0.46 μm for a single layer of rGO on PVDF to 0.62 μm for five layers (shown in **Fig.2b-d**). It is noteworthy that rough surfaces may lead to insufficient contact between the electrodes and high-viscosity gel polymer electrolyte, as the viscous materials are less able to fill the tiny gaps and indentations on the electrodes' surface, which could potentially affect the efficiency of ion contact and transmission.

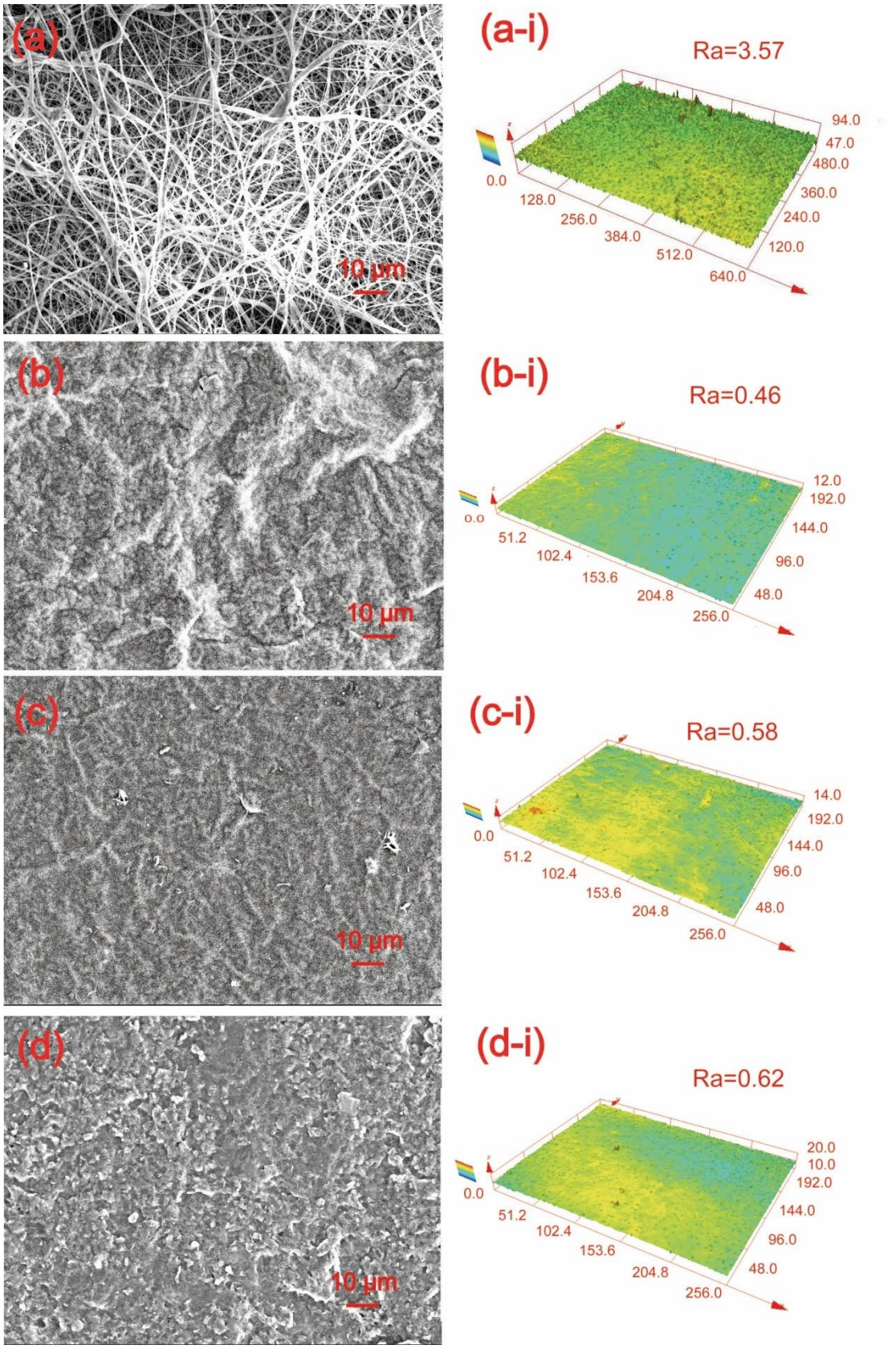

Figure 2. SEM images of the (a) PVDF, (b) 1rGO/PVDF, (c) 3rGO/PVDF, (d) 5rGO/PVDF electrodes, and (a-i)-(d-i) display the corresponding confocal images.

5.1.2 EDX analysis of rGO-printed PVDF films

EDX analysis was utilized to determine the ratio of carbon to oxygen (C/O) in GO and rGO. According to **Fig. 3a** and **3b**, the C/O ratios for 5GO/PVDF and 5rGO/PVDF are 4.75 and 9.32, respectively. The lower ratio in GO can be attributed to its abundant oxygenated functional groups. During the in-situ reduction of GO to rGO within the printing process, many of these oxygen-containing groups are eliminated, thus increasing the C/O ratio. This change, as confirmed by EDX analysis, signifies the transformation from GO to rGO.

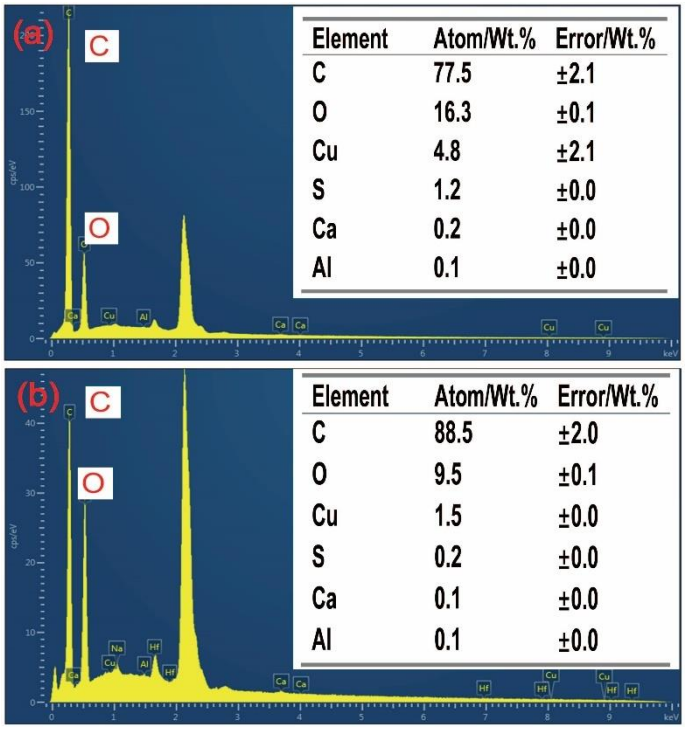

Figure 3. EDX spectra of (a) 5GO/PVDF and (b) 5rGO/PVDF

5.1.3 Surface resistance of rGO-printed PVDF films

Fig.4 illustrates a gradual reduction in the surface resistance of the (rGO printed layers, which stabilizes after five print passes. The layers washed with water display significantly reduced surface resistance relative to those that were not washed. This reduction is attributed to the removal of organic residues, solvents, and unreacted precursors from the rGO layers during the washing process. Specifically, the surface resistance of the rGO layer, after five printing passes and washing, was measured at 157,438 Ω/sq. Given that the relationship between resistance and capacitance is not strictly predictable, and an increase in capacitance is not invariably associated with a decrease in resistance, this research focused on exploring the ideal number of print layers. To this end, PVDF membranes with 1, 3, and 5 layers of rGO were selected for detailed examination to identify the best layer configuration for compatibility with supercapacitors.

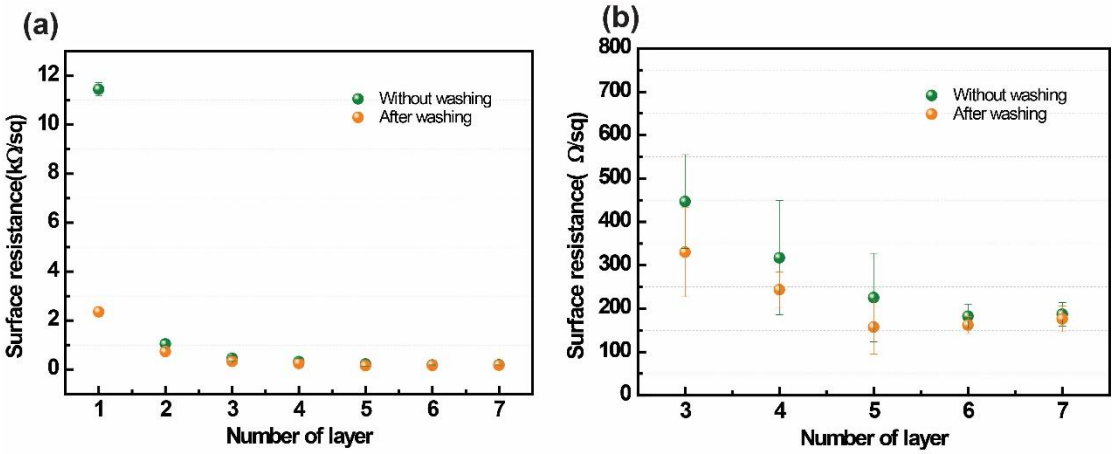

Figure 4. Surface resistance of (a) rGO layers printed on PVDF membrane without and after washing and (b) magnification with different number of printing passes

5.1.4 XPS analysis of rGO-printed PVDF films

The XPS spectra were employed to analyze the chemical states across all samples, with findings depicted in **Fig. 5**. Given the limited penetration depth of XPS, typically just a few nanometers, it's improbable that the substrate affected the outcomes. As a precaution, XPS scans were also performed on the PVDF film. The broad-scan XPS spectra of PVDF reveal the presence of C1s at 286.14 eV, F1s at 688.06 eV, and O1s at 532.32 eV. **Table 1** shows that the survey spectra of GO indicated a carbon-to-oxygen (C/O) atomic ratio of 2.39, 2.61, and 2.15 for 1GO/PVDF, 3GO/PVDF, and 5GO/PVDF, respectively. For rGO, this ratio increased to 3.54, 3.67, and 3.81 for 1rGO/PVDF, 3rGO/PVDF, and 5rGO/PVDF, respectively, suggesting the removal of oxygen groups during the in-situ reduction process.

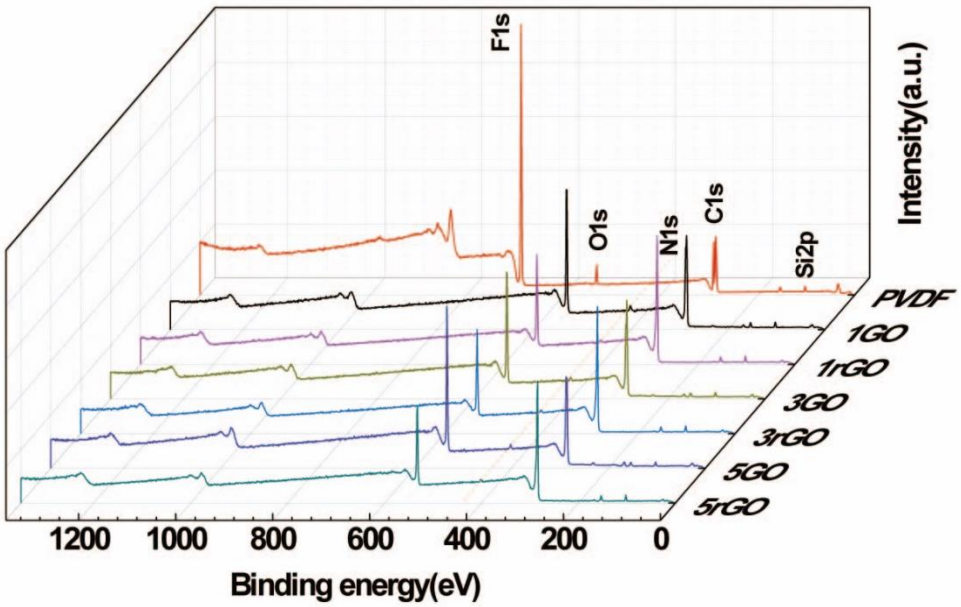

Figure 5. The XPS wide-scan spectrum of all the films

Table 1. Surface atomic concentrations in GO/PVDF, rGO/PVDF and PVDF

Sample	Concentration (at%)-(BE (eV))					
	C (286.14)	O (532.32)	N (400.90)	Si2p (102.10)	S2p (167.81)	F (688.06)
1GO/PVDF	65.51	27.44	3.40	2.60	1.05	−−
1rGO/PVDF	73.11	20.65	2.83	3.41	−−	−−
3GO/PVDF	68.23	26.17	1.94	2.48	1.18	−−
3rGO/PVDF	74.71	20.36	1.83	3.10	−−	−−
5GO/PVDF	63.98	29.80	2.41	2.35	1.46	−−
5rGO/PVDF	75.27	19.77	1.38	3.01	0.58	−−
PVDF	51.85	4.00	−−	2.79	−−	41.35

To delve deeper into the analysis, the C1s XPS spectra of the samples were further explored. As illustrated in **Fig. 6a** and **6b**. The C1s XPS spectra for GO were decomposed into four distinct peaks, each linked to carbon species displaying varying chemical valences: these include the non-oxygenated ring C=C at 284.57 eV, the C-O bond at 286.67 eV, the carbonyl group C (C=O) at 287.88 eV, and the ester bond C(O)O at 288.79 eV. **Table 2** provides the ratios of the peak areas for these carbon bonds relative to the total area, as determined from the XPS data. It is apparent that the proportions of the area associated with oxygenated functional groups (C-O, C=O, and C(O)O) were approximately 65.24%, 59.69%, and 51.55% for 1GO/PVDF, 3GO/PVDF, and 5GO/PVDF respectively. In contrast, these percentages fell to 39.88%, 43.30%, and 44.99% for 1rGO/PVDF, 3rGO/PVDF, and 5rGO/PVDF, signalizing the effective reduction of GO. Within the GO spectra, the peak at 530.77 eV is attributable to C-OH, while the peaks at 531.77 eV and 532.92 eV are associated with C-O and O=C-OH/C=O groups, respectively. The reduction treatment across the rGO samples resulted in a diminished C-O content, indicating a reduction in oxygen functional groups and a shift towards the properties of pristine graphene.

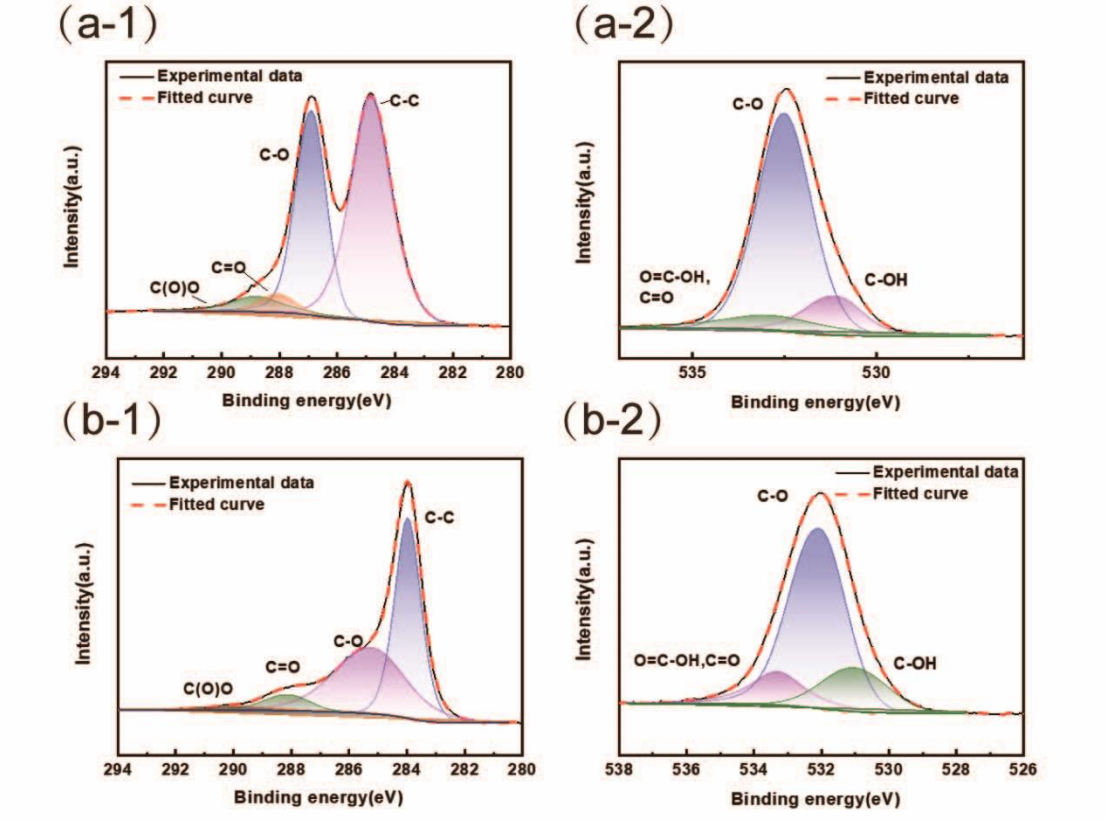

Figure 6. High resolution C1s XPS fitting curves of 5GO/PVDF, and high resolution O1s XPS fitting curves of 5rGO/PVDF

Table 2. Atomic contents of C and O chemical groups in GO/PVDF and rGO/PVDF.

Sample	C 1s group content (at%)–(BE (eV))			
	C-C (284.57)	C-O (286.67)	C=O (287.88)	C(O)O (288.79)
1GO/PVDF	34.75	37.51	13.03	14.70
1rGO/PVDF	60.12	28.20	9.79	1.89
3GO/PVDF	40.31	38.02	5.67	16.00
3rGO/PVDF	56.71	32.32	5.74	5.24
5GO/PVDF	48.45	43.17	6.17	2.21
5rGO/PVDF	55.01	36.48	3.52	4.99
Sample	O 1s group content (at%)–(BE (eV))			
	C-OH (530.77)	C-O (531.77)	O=C-OH, C=O (532.92)	
1GO/PVDF	14.18	68.67	17.14	
1rGO/PVDF	14.39	59.48	26.13	
3GO/PVDF	9.83	83.43	6.73	
3rGO/PVDF	10.07	61.50	28.43	
5GO/PVDF	14.27	75.05	10.68	
5rGO/PVDF	18.42	68.00	13.58	

5.1.5 Electrochemical characterizations of rGO-printed PVDF films

Fig. 7 displays the CV curves for rGO/PVDF electrodes, spanning a voltage range of -0.5V to 0.5V and a scan rate from 10 to 200 mV/s. The curves (**Fig. 7a-c**) at lower scan rates exhibit a nearly perfect rectangular shape, demonstrating characteristic electric double-layer capacitive behavior. With an increase in scan rate, the curves remain quasi-rectangular, showcasing the

electrodes' excellent capacitive properties and reversibility. Furthermore, as scan rates rise, there is a noticeable increase in both the current peak and the area under the CV curves, indicating robust rate performance. **Fig. 7d** demonstrates that at a 10 mV/s scan rate, the 1rGO/PVDF electrode exhibits the highest capacitance at 85.66 F/g, substantially surpassing the 53.81 F/g and 25.58 F/g of the 3rGO/PVDF and 5rGO/PVDF, respectively.

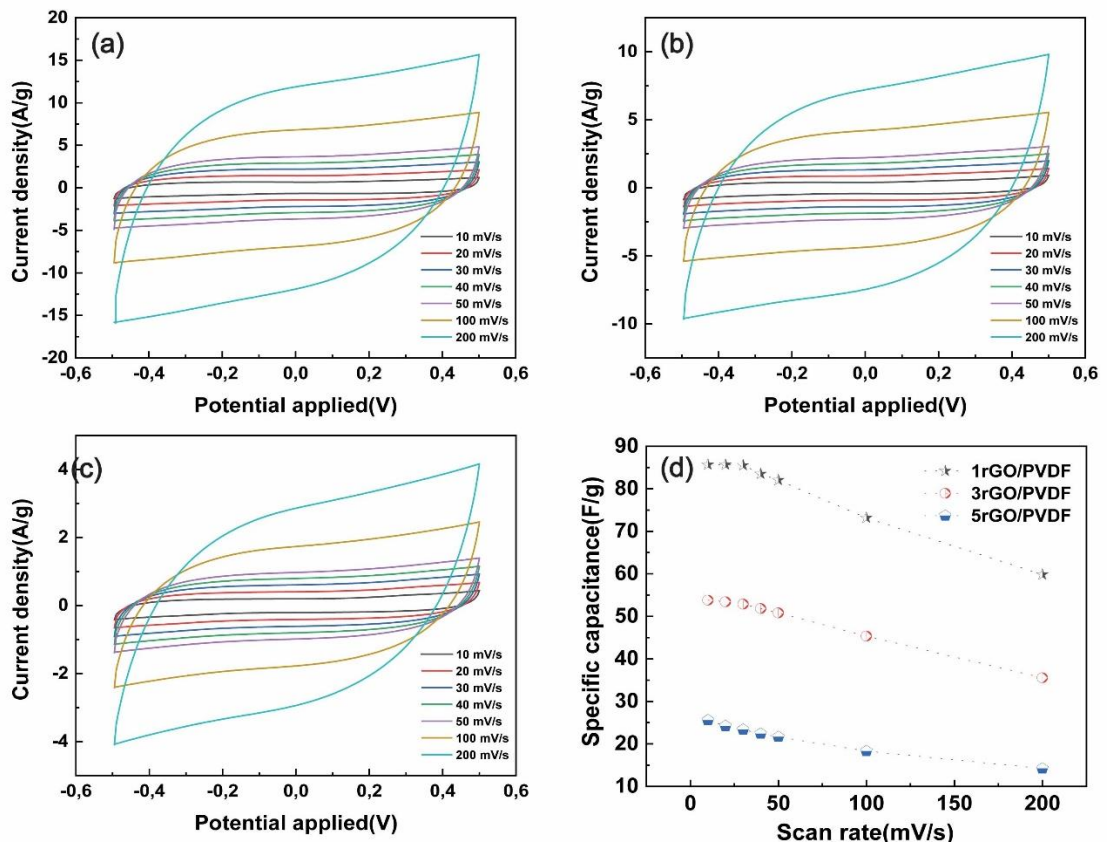

Figure 7. The CV curves of (a)1rGO/PVDF, (b) 3rGO/PVDF, (c) 5rGO/PVDF across varied scan rates, and (d) the specific capacitance of various rGO/PVDF electrodes as determined at different scan rate

To evaluate the flexibility of the electrode, 1rGO/PVDF was attached to cylindrical substrates with radii of 4, 6, and 8 mm, as depicted in **Fig. 8**. This experiment aimed to simulate conditions where the electrode might be used in flexible electronics, which often require substantial bending. The results were promising, showing minimal impact on the electrode's capacitive behaviour despite the physical bending. The CV curves remained consistently quasi-rectangular in both bent and flat configurations. This pattern demonstrates the electrode's excellent ability to retain charge storage and efficiency under mechanical stress, making it highly suitable for use in flexible and wearable electronic devices where durability and performance under deformation are crucial.

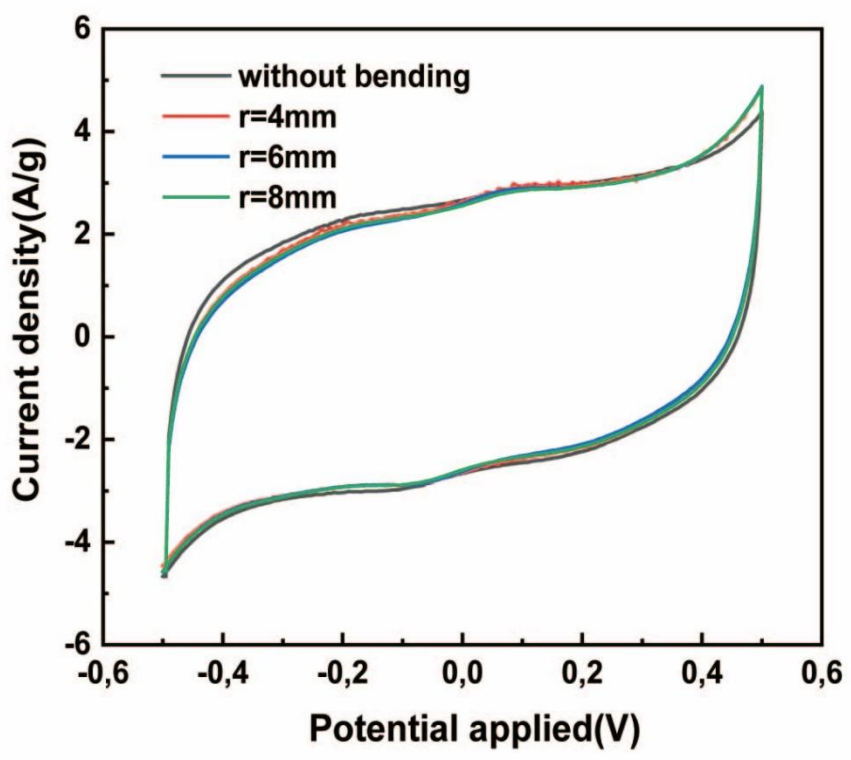

Figure 8. the CV responses of both flat and bent configurations of 1rGO/PVDF at bending radii of 4 mm, 6 mm, and 8 mm, measured at a scan rate of 40 mV/s, 1-electrode, 2-cylindrical pieces.

To conduct a thorough evaluation of the electrochemical characteristics of the rGO/PVDF electrode, we also performed charge/discharge tests across a voltage range of 0 to 0.8 V at various current densities, as depicted in **Fig. 9a-c**. The charge/discharge curves showed notable symmetry between the anodic charging and cathodic discharging segments, indicating a high level of reversibility typical of standard capacitive materials. This finding aligns with earlier observations from cyclic voltammetry studies, as noted in the literature [18]. An inset in **Fig. 9d** presents specific capacitance curves, calculated at current densities ranging from 2 A/g to 10 A/g, where the peak specific capacitance achieved was 83.29 F/g after applying one layer of rGO ink. It was observed that the specific capacitance values derived from these GCD curves were marginally lower than those recorded from CV measurements, consistent with previously reported results [19]. Moreover, these capacitance curves displayed a decreasing trend with increasing current densities, a phenomenon attributable to the faster charge/discharge rates at higher currents. As the current density increases, there is inadequate time for the electrolyte ions to fully permeate the porous structure of the electrode, resulting in less effective utilization of the available surface area and, consequently, a decrease in capacitance[20].

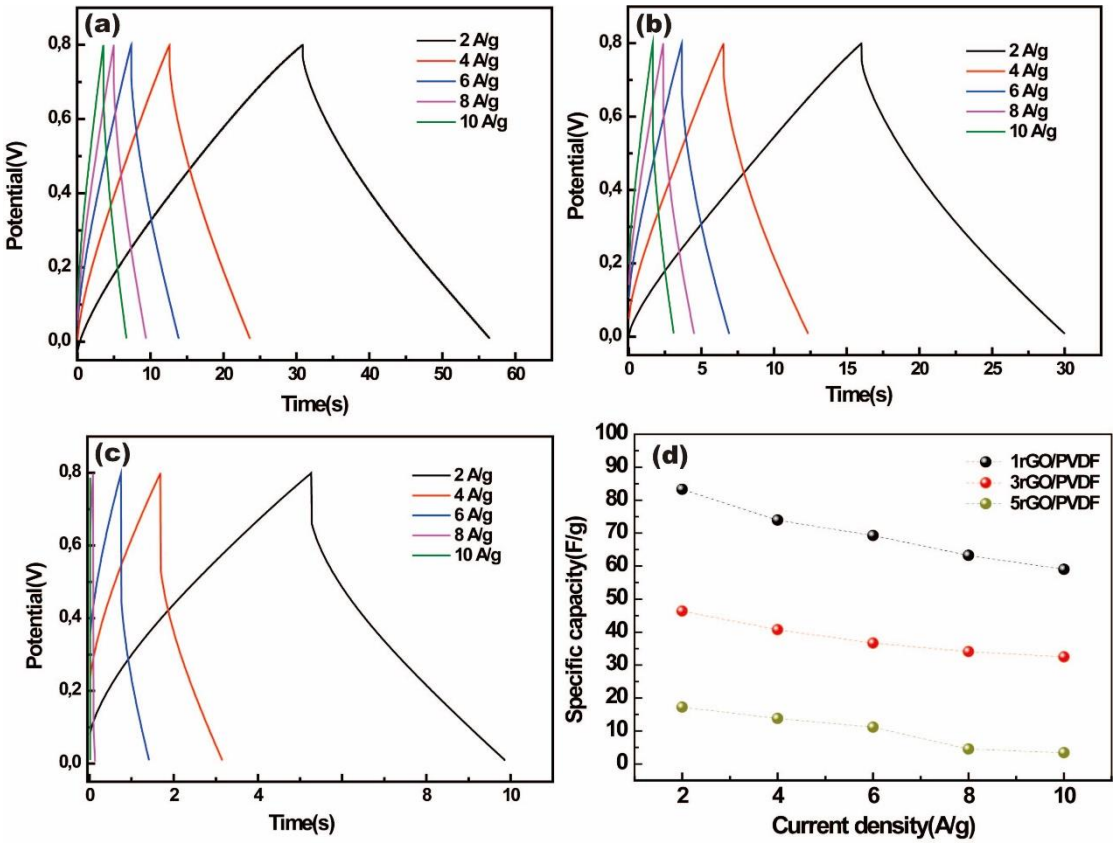

Figure 9. GCD curves of (a) 1rGO/PVDF (b) 3rGO/PVDF, and (c) 5rGO/PVDF electrode, (d) the specific capacitance of different rGO/PVDF electrodes calculated at different current density.

It was observed that electrodes featuring a single layer of rGO demonstrated markedly higher specific capacitance than those constructed with three or five layers. This disparity is likely attributable to the dynamic interaction between electrode thickness and electrolyte diffusion efficacy. Given that PVA is a long-chain polymer, it encounters difficulties in permeating the dense pore network of electrodes due to the substantial size of its molecular chains. The complex entanglement of these chains, coupled with the hydrogen bond interactions at the pore surfaces, poses a barrier to their entry at the pore openings. Further complications arise once the chains manage to infiltrate the pore structure, as interactions with internal pore molecules may obstruct deeper penetration, as referenced in the literature [21].

Additionally, during the fabrication of double-layer capacitors through solvent evaporation, the contraction of electrolyte volumes can lead to incomplete filling, as depicted in **Fig. 10** [22]. Consequently, as the number of printed layers increases, leading to greater electrode thickness, the lack of sufficient electrolyte penetration hampers the full saturation of the electrode structure. This deficiency in electrolyte filling adversely affects the electrode's charge storage capabilities, culminating in reduced performance metrics such as specific capacitance and energy density.

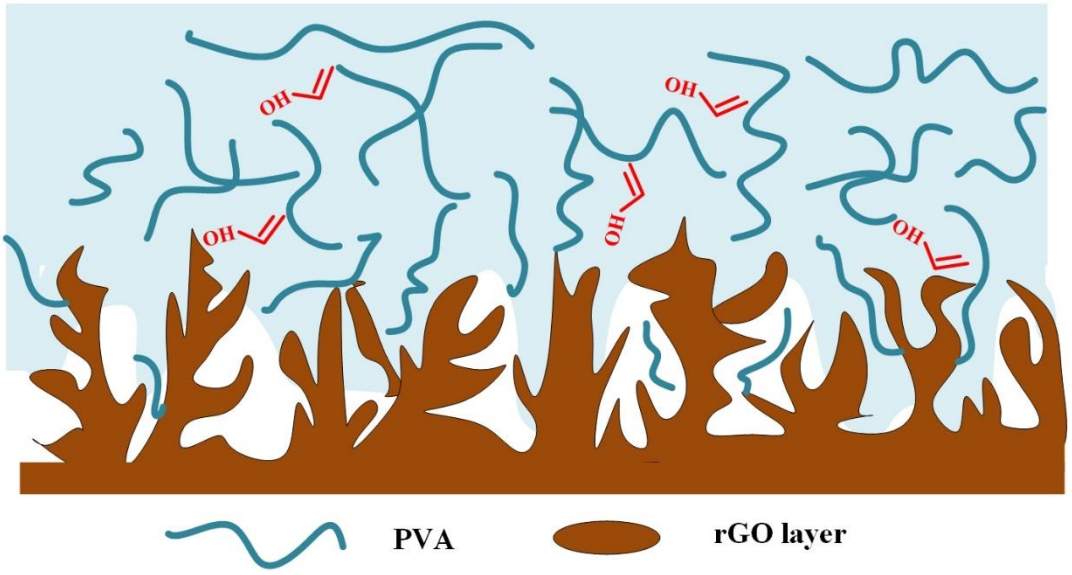

Figure 10. Schematic of the infiltration of PVA into the porous rGO electrode

In evaluating the operational electrochemical performance, the emphasis on the electrode's cycling stability becomes paramount. The 1rGO/PVDF electrode underwent cycling tests at a charge/discharge current density of 2 A/g, where it exhibited robust cycling durability as illustrated in **Fig. 11.** Notably, this electrode maintained 93% of its efficiency following 4000 charge-discharge cycles at the specified current density of 2 A/g, thereby indicating its superior electrochemical stability.

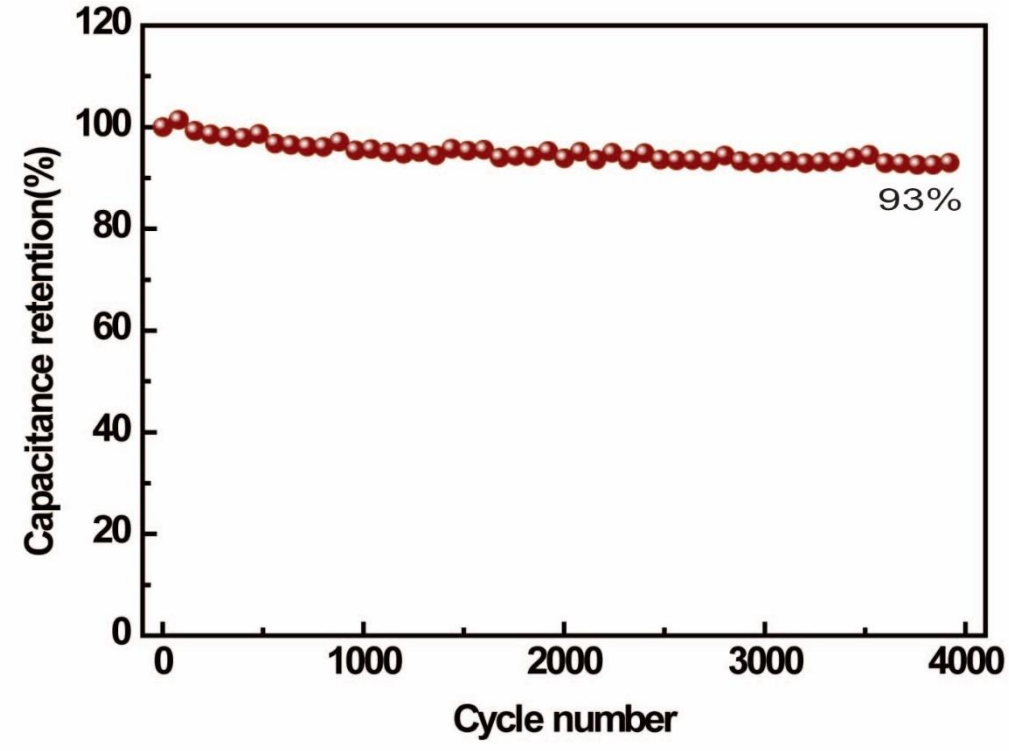

Figure 11. Cycle stability of the 1rGO/PVDF electrode tested at a current density of 2 A/g

Electrochemical impedance spectroscopy (EIS) is a highly beneficial instrument to basically comprehend the electrochemical behaviours of rGO/PVDF electrodes at the bulk and interface according to the equivalent circuit models, which are composed of resistive and capacitive elements. The data from EIS was depicted as a Nyquist diagram, presenting the frequency-dependent characteristics of the electrode/electrolyte interface through a graphical representation that contrasts the impedance's real and imaginary parts[23]. The Nyquist plot demonstrated a strong correspondence to the equivalent circuit depicted in **Fig. 12a**, as described by the subsequent formula (7) [24].

$$z = R_S + \frac{1}{j\omega C_{DL} + \frac{1}{R_{CT} + W_o}} - j\frac{1}{\omega C_F} \qquad (7)$$

where R_s (ESR) is bulk resistance, j is the imaginary unit, ω is the angular frequency, C_{DL} is the double-layer capacitance, R_{CT} is the charge transfer resistance, W_o is the finite-length Warburg diffusion element, C_F is the faradaic capacitance. By Nyquist curve fitting, the estimated values of R_s , R_{CT}, C_{DL}, and C_F can be obtained as 64.27Ω, 25.26 Ω, 95.44 F/g and 0.13 F/g, respectively.

The EIS measurements obtained are further evaluated by examining the Bode phase angle diagram, which displays the fluctuation in phase angle with respect to the frequency applied. A phase angle of 90° is indicative of the material's perfect capacitive nature, whereas any other value points to pseudocapacitive properties [25]. As indicated by **Fig. 12b**, the phase angle nears 80° in the low-frequency zone, suggesting predominantly electric double-layer charge retention traits alongside a fractional presence of faradaic charge retention activity within the electrode.

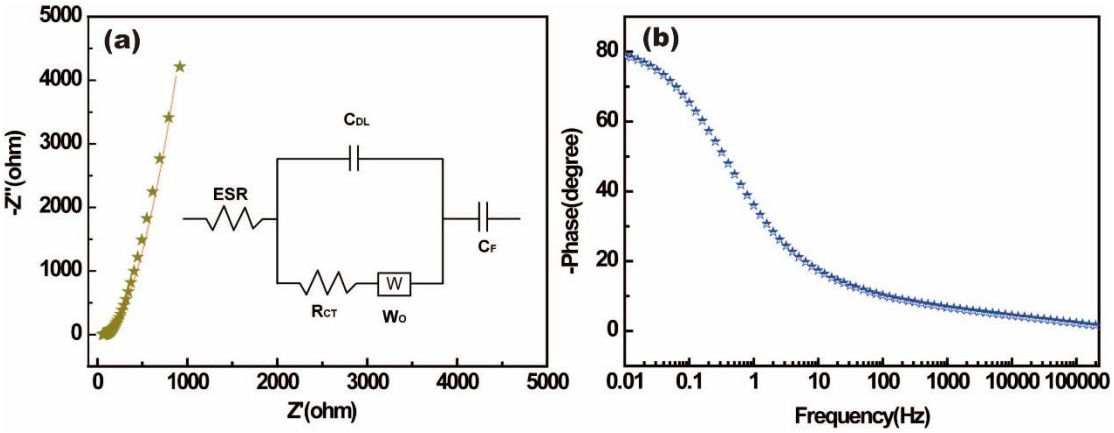

Figure 12. (a) Nyquist diagram for the 1rGO/PVDF electrode, covering frequencies from 100 kHz down to 0.01 Hz. (b) Bode phase angle plot of the 1rGO/PVDF.

The Ragone chart is utilized to illustrate the performance of rGO/PVDF as electrode materials in **Fig. 13** and **Table 3**, alongside the data from existing publications. It is significant to highlight that the energy storage capacity reaches 7.5 Wh/kg with an electrical output of 1.04 kW/kg at an electric charge flow rate of 2 A/g and 5.3 Wh/kg at an elevated electrical output of 6.0 $kWkg^{-1}$ when the charge flow rate is increased to 10 A/g. Relative to electrodes cited in scholarly articles regarding electrospun carbon nanofibers (CNFs) and carbon nanotubes (CNTs), our electrode outstrips most of the formerly described electrode carbons, especially when operating under conditions demanding high power output. Although CNFs devices demonstrate a superior energy storage capacity compared to our model, their battery-like

electrochemical behaviour, characterized by lower power output, could diminish their appeal in the marketplace as an emerging commercial product.

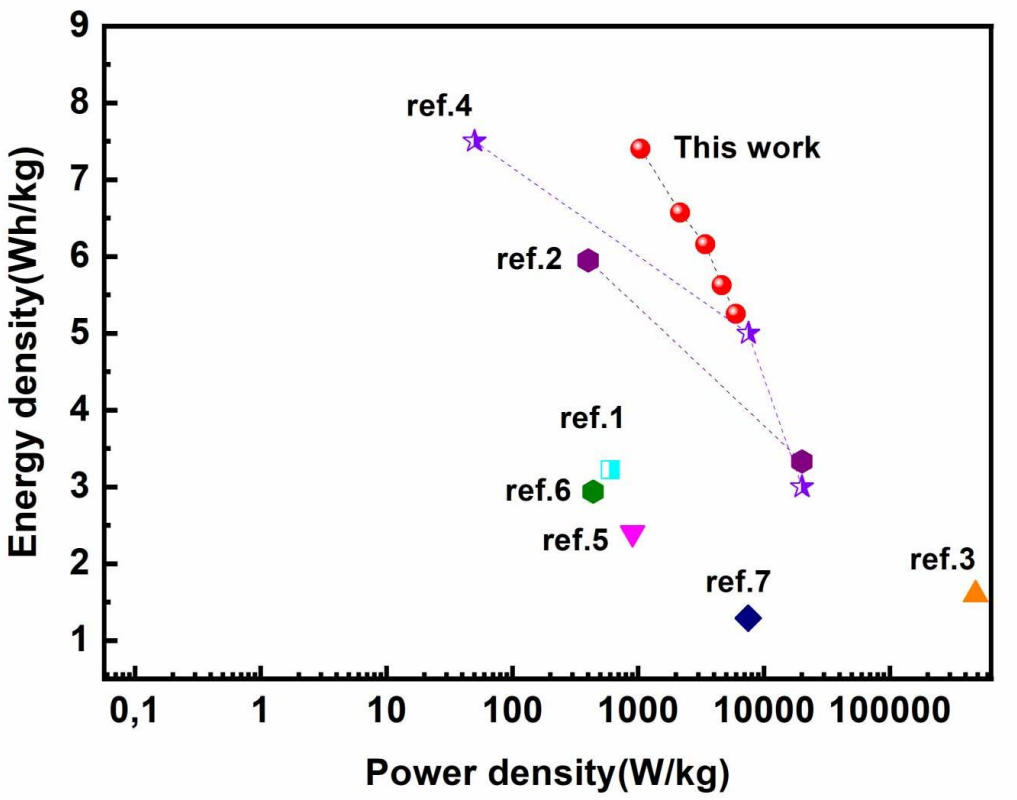

Figure 13. Ragone plot of the 1rGO/PVDF for the energy density and power density of the fabricated device compared with the reported literatures.

Table 3. The reported literatures shown in the Ragone plot

Number of references	Techniques and materials	reference
ref.1	Electrospinning freestanding PCNFs nanofibers	[26]
ref.2	Electrospinning hybrid CCNFs	[27]
ref.3	Reactively sputtered TiN	[28]
ref.4	Electrospinning PVP templated CNFs	[29]
ref.5	Chemical vapor deposited CNT transparent sheets	[30]
ref.6	Solid carbon source converted graphene	[31]
ref.7	In_2O_3 nanowire/CNT heterogeneous films	[32]

5.2 In-situ reduced Ag/rGO printed PP flexible supercapacitor

5.2.1 SEM characterization of Ag/rGO printed PP films

The group of SEM images illustrates the microstructural characteristics of the materials' surfaces. **Fig. 14a** shows an untreated PP spun-bonded nonwoven fabric, revealing its characteristic fibrous network. The fiber lumps could be a result of the entwining and thermal pressing during the production process [33]. **Fig. 14b** shows the rGO layer that has been inkjet-printed on the PP nonwoven fabric, showing complete coverage of the PP by the rGO. Appretan® N 9415 is used as a pre-coating to achieve a smoother surface, which improves the

adhesion of ink onto the nonwoven fabric. The formation of 'ridges' visible in the image is likely due to the coffee ring effect as the solvent of ink evaporates [5]. **Fig. 14c** shows the 4Ag/rGO active layer created by a one-step in situ reduction method, with 'snowflake' shaped AgNPs indicated by yellow arrows, and these are further enlarged in **Fig. 14d**. These AgNPs enhance electrical connectivity and expand the active surface area of the electrode, which is advantageous for boosting the electrochemical performance of the electrode, potentially increasing charge-discharge efficiency, current density, and extending cycle life in supercapacitors. Lastly, **Fig. 14e** and its detailed counterpart, **Fig. 14f**, were taken using the angle-sensitive backscatter (AsB) electron signal mode, which is particularly effective for detecting metallic particles such as the silver particles in the images. In AsB mode, these particles appear exceptionally bright due to the increased production of backscattered electrons from their higher atomic number. Furthermore, the AsB detector provides a greater depth of field compared to the InLens electron detector, which is especially beneficial for analyzing heterogeneous samples[34].

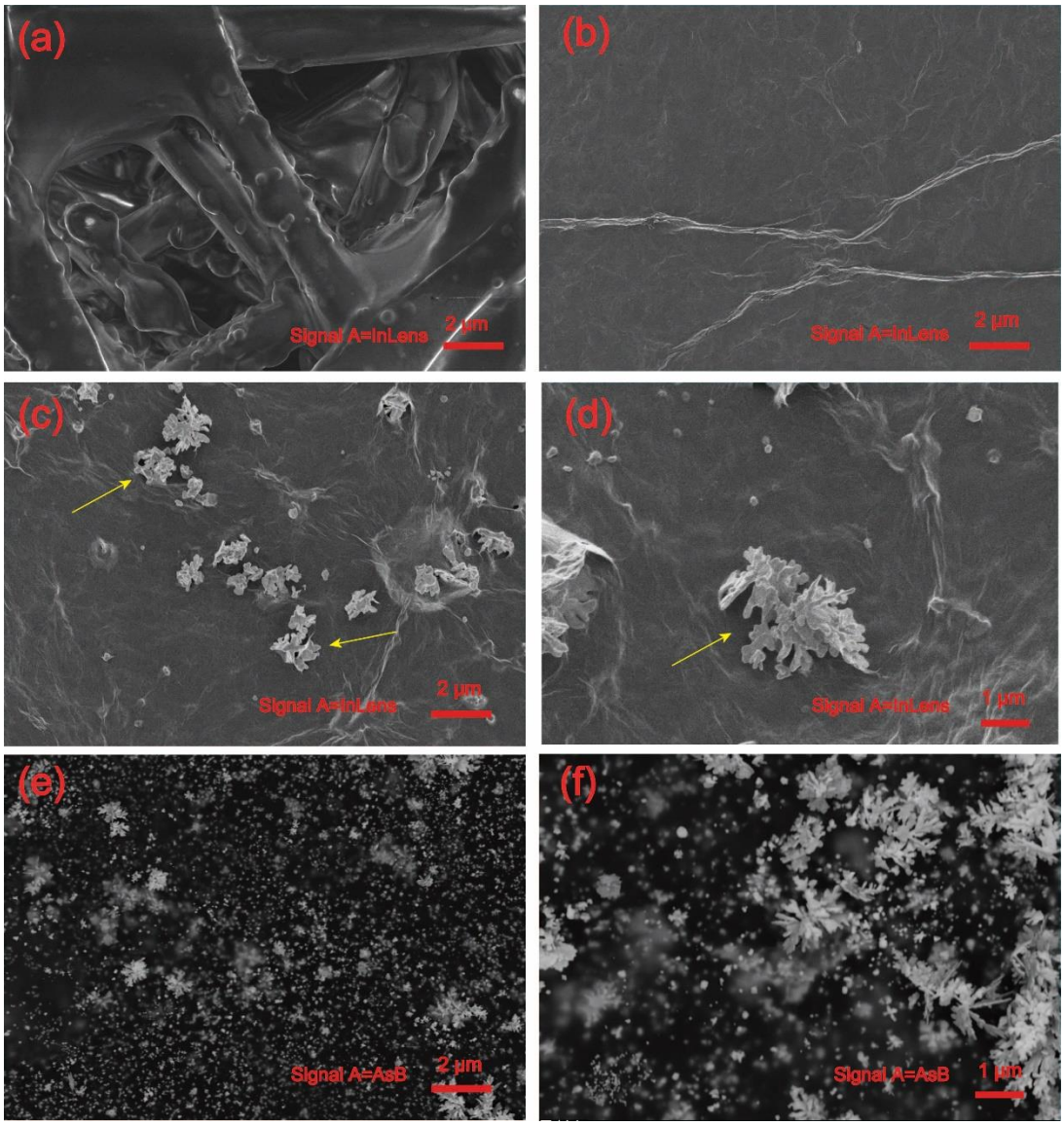

Figure 14. SEM images of the (a)pure PP nonwoven, (b)rGO, (c) 4Ag/rGO under InLens electron signal detection mode, (d) the magnification of 4Ag/rGO under InLens, (e) 4Ag/rGO

under AsB detector electron signal detection mode, and (f) the magnification of 4Ag/rGO under AsB.

5.2.2 EDX analysis of Ag/rGO printed PP films

From **Fig. 15**and **Table 4**, it is evident that the rGO electrode mainly consists of carbon (C) and oxygen (O), with traces of sulphur (S) present. Meanwhile, the 4Ag/rGO specimen not only contains C and O but also a substantial presence of Ag, as shown clearly in the EDS map. According to the EDX spectra, the mass ratio of the Ag component reached 29.62%. The even distribution of AgNPs achieved through an environmentally friendly in-situ reduction technique known as RIP plays a vital role in improving the functionality of flexible high-performance supercapacitor electrodes.

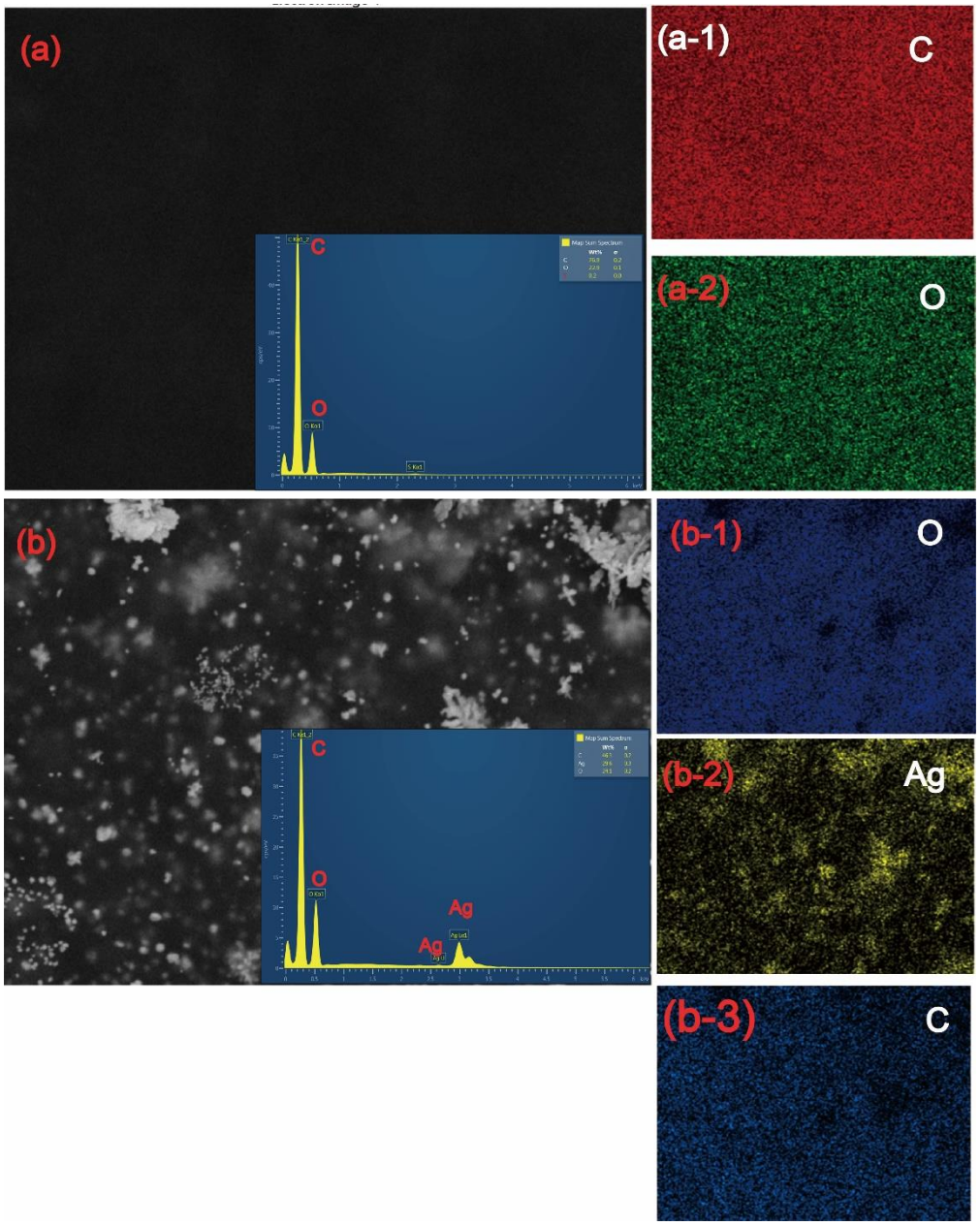

Figure 15. SEM-EDX elemental mapping of the (a) rGO and (b) 4Ag/rGO electrodes, and the inset is the respective EDX spectra

Table 4. Quantification results of EDX spectra

Element	rGO		4Ag/rGO	
	Wt%	Atomic %	Wt%	Atomic %
C	76.87	81.65	46.33	68.45
O	22.91	18.27	24.05	26.68
S	0.22	0.09	/	/
Ag	/	/	29.62	4.87

5.2.3 Surface resistance of Ag/rGO printed PP films

Fig. 16a clearly demonstrates a pattern in which the surface resistance of the electrode significantly reduces as the concentration of $AgNO_3$ in the composite electrode increases. Silver is well-known for its exceptional conductivity and the AgNPs reduced in situ enhance the overall electrical conductivity of the electrodes. However, this decrease in surface resistance is not linear and exhibits a threshold effect. Specifically, there is a marked decline in resistance when the $AgNO_3$ concentration increases from 0.25 mg/ml to 0.625 mg/ml. Beyond 0.5 mg/ml, the decrease in resistance becomes more gradual.

Moreover, the optical images presented in **Fig. 16b** and **16c** illustrate that the luminance of a small light bulb remains nearly consistent regardless of whether the Ag/rGO electrode is flat or bent. This observation confirms the robust stability of the electrode's resistance across different bending states, showcasing its potential for flexible electronic applications.

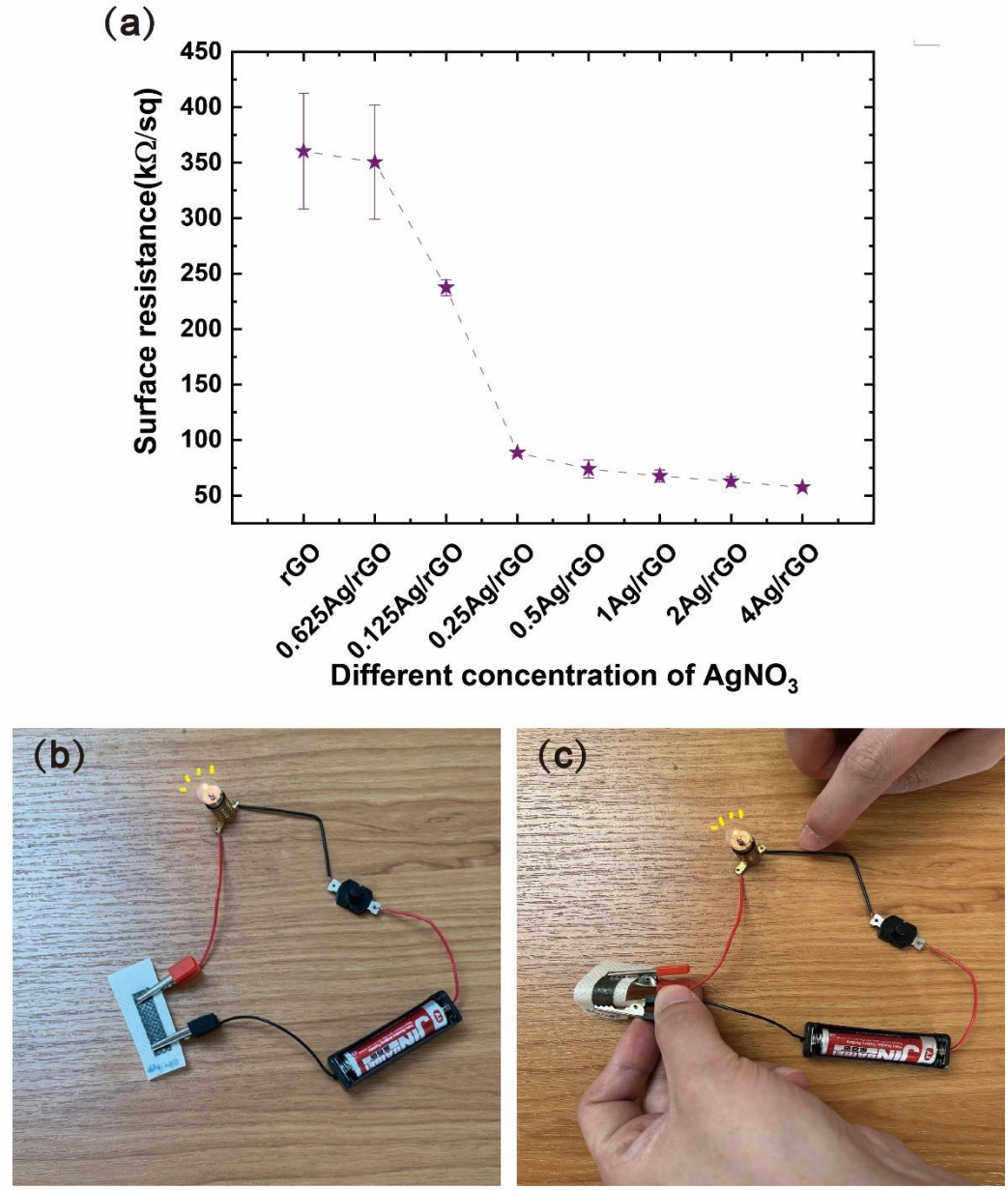

Figure 16. (a) Surface resistance of electrodes prepared with different concentrations of $AgNO_3$, (b) optical photo of resistivity of 4Ag/rGO at different bending states.

5.2.4 XPS analysis of Ag/rGO printed PP films

The elemental makeup and oxidation states can be determined using XPS analysis. XPS also proves to be an effective instrument for measuring the reduction level of rGO. In the overview spectrum shown in **Fig. 17a** and **Table 5**, both rGO and 4Ag/rGO electrodes displayed characteristic peaks for C1s and O1s at 284 eV and 530 eV, respectively, with an additional peak at 372 eV. Notably, N1s peaks were exclusive to the 4Ag/rGO sample. This occurrence might stem from the inkjet printing reduction process, where the nitrate NO_3^- from $AgNO_3$ could be partially converted to ammonia (NH_3) or other nitrogen-based compounds, which then remain on or integrate into the active layer either as dopants or through adsorption.

It is crucial to recognize that in the fabricated 4Ag/rGO electrode, besides the C1s and O1s peaks, a separate XPS peak for Ag 3d was also observed. To verify the oxidation state of silver

in the 4rGO/Ag electrodes, the detailed XPS spectrum of Ag 3d is shown in **Fig. 17b** and **Table 6**. Clearly, two peaks at 368 eV and 374 eV are visible in the 4rGO/Ag composites, indicative of the metallic states Ag^0 $3d_{5/2}$ and Ag^0 $3d_{3/2}$, respectively. This confirms that silver exists in its metallic form on the electrode surface, suggesting that Ag nanoparticles are incorporated into the active layer, rather than Ag^+ ions, and remain stable in an air-exposed environment[35].

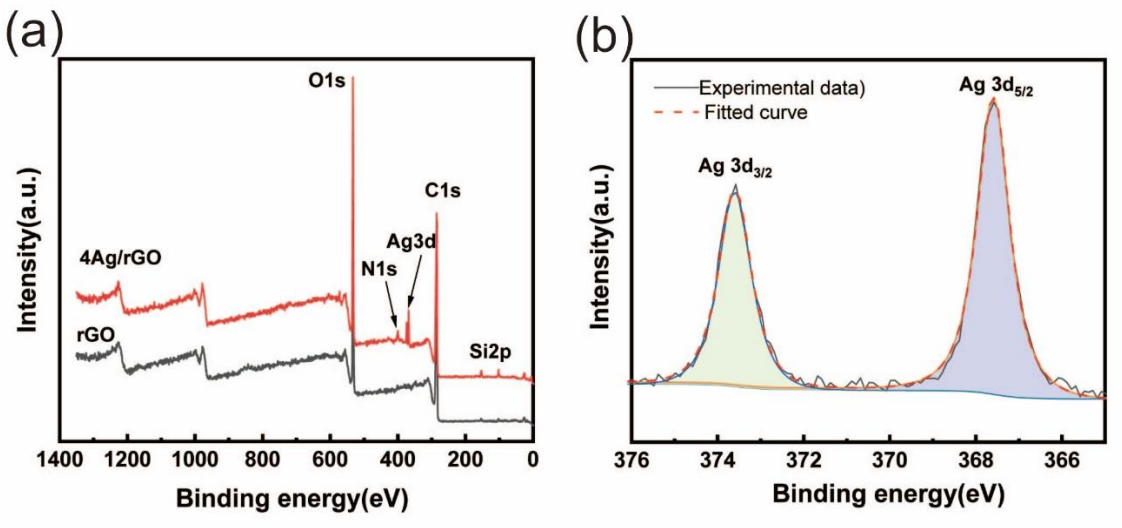

Figure 17. The XPS wide-scan spectrum of all the electrodes. (b) high resolution of Ag XPS fitted curves of 4Ag/rGO

Table 5. Surface atomic concentrations in different electrodes

Sample	Concentration (at%)				
	O (530 eV)	C (284 eV)	N (401 eV)	Ag (374 eV/368 eV)	Si2p (99 eV)
rGO	26.78	73.15	/	/	0.07
4Ag/rGO	32.20	67.11	/	0.58	0.11

The C1s XPS spectra for rGO and 4Ag/rGO, as shown in **Fig. 18a** and **18c**, can be resolved into three peaks originating from C-C/C=C (284 eV) in the aromatic ring, C-O (286 eV) from epoxy and alkoxy structures, and C=O/O-C=O (289 eV) groups, respectively [36]. Similarly, as depicted in **Fig. 18b** and **18d**, the O1s XPS spectra can be resolved into peaks for C=O (532 eV) and C-O-C/C-OH (531 eV) [37]. From **Table 5**, it is important to note that the C/O ratio for Ag/rGO is 2.08, considerably lower than the 2.73 C/O ratio for rGO, which may be attributed to the creation of specific adsorptive sites by AgNPs on the electrode's surface. These sites could differentially affect the elimination of oxidized functional groups during the reduction process.

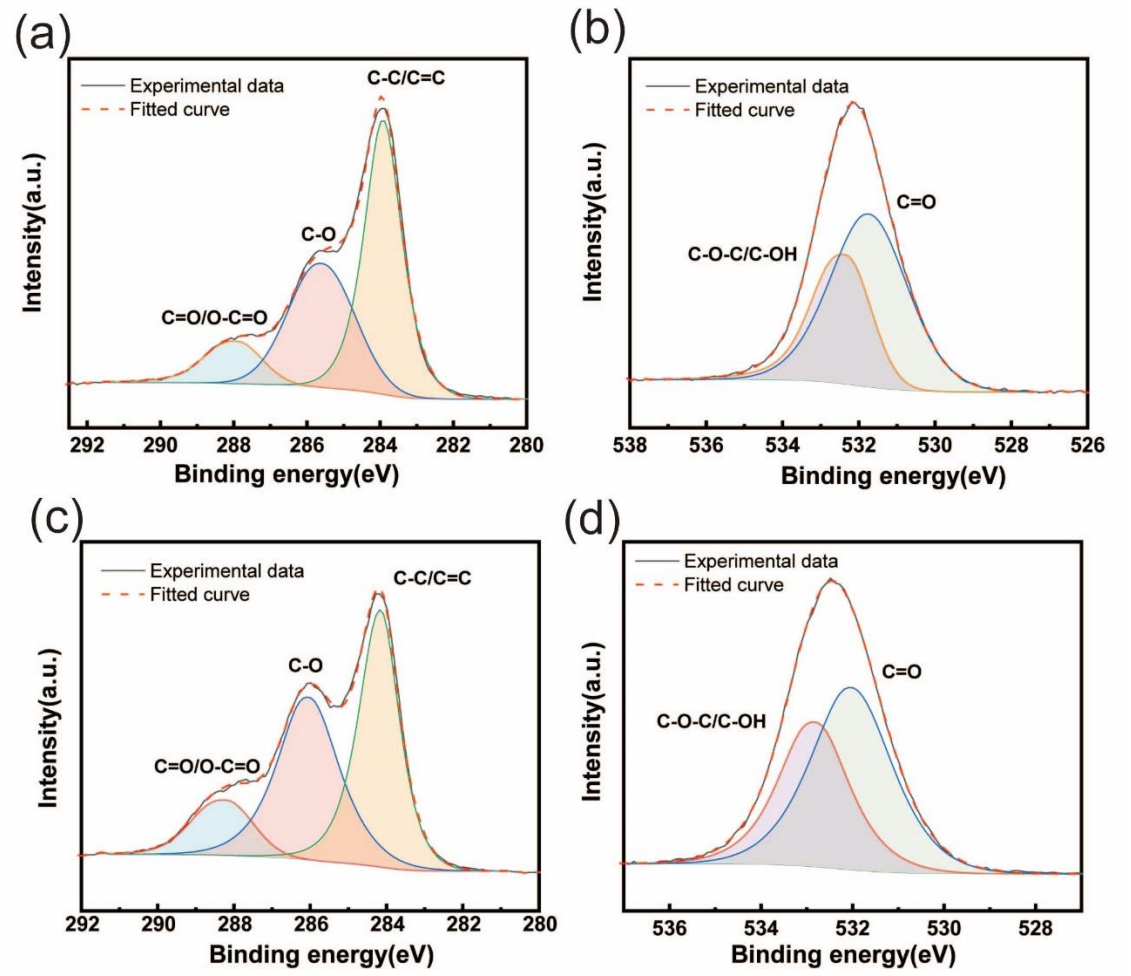

Figure 18. (a), (c) are high resolution C1s XPS fitted curves of rGO and 4Ag/rGO. (b), (d) are high resolution O1s XPS fitted curves of rGO and 4Ag/rGO.

Table 6. Atomic contents of C, O, and Ag elements in various electrodes

Sample	C 1s group content (at%)			O 1s group content (at%)		Ag content (at%)	
	C-C/C=C (284 eV)	C-O (286 eV)	C=O/O-C=O (289 eV)	C-O-C/C-OH (531 eV)	C=O (532 eV)	$3d_{3/2}$ (368 eV)	$3d_{5/2}$ (374 eV)
rGO	56.46	33.52	10.02	26.59	73.41	/	/
4Ag/rGO	45.59	43.21	11.20	23.44	76.56	37.00	63.00

5.2.5 Electrochemical characterizations of Ag/rGO printed PP films

Apart from the pure rGO electrode, the CV traces in **Fig. 19a** and **19b**, recorded at a scan rate of 10 mV/s for assorted electrodes, exhibit clear redox peaks. Owing to the incorporation of AgNPs in these electrodes, the redox behavior of Ag/Ag^+ relative to Ag/AgCl manifests an anodic peak alongside a cathodic peak, with the current ratio of these peaks (I_{pa}/I_{pc}) being roughly one, distinctly confirming that the redox activity of AgNPs on the hybrid electrode is reversible. This is a typical indication of pseudocapacitive characteristics [38]. The diagram in **Fig. 19c** displays the specific capacitance of electrodes at various $AgNO_3$ concentrations. The corresponding curve indicates that as the $AgNO_3$ concentration increases, there is a preliminary

increase in specific capacitance, which subsequently decreases upon surpassing the optimum concentration (near 4 mg/ml, where the specific capacitance attains 800.30 F/g). The rise in capacitance is due to the synergistic interaction between the intense redox properties of AgNPs (participating in Faradaic reactions, e.g., pseudocapacitance) and their notable electrical conductivity (supporting non-Faradaic actions, e.g., electric double-layer capacitance).

Conversely, the decline in capacitance can be ascribed to the agglomeration of AgNPs, which diminishes the accessible surface area for redox activities and increases internal resistance. Moreover, the considerable weight of silver relative to graphene implies that while adding silver boosts the overall capacitance of the composite electrode, it could reduce the specific capacitance due to a significant rise in the mass of the electrode. Additionally, the GCD profiles in **Fig. 19d**, at a steady current density of 0.25 mA/cm², illustrate the charge and discharge dynamics of the electrodes. It is noted that the GCD trace displays significant plateaus during the charging or discharging periods, a characteristic of battery-like behavior. These plateaus signify the voltage remaining fairly constant while faradaic reactions unfold, differing from the constant rise or drop in voltage typical of purely capacitive processes [39].

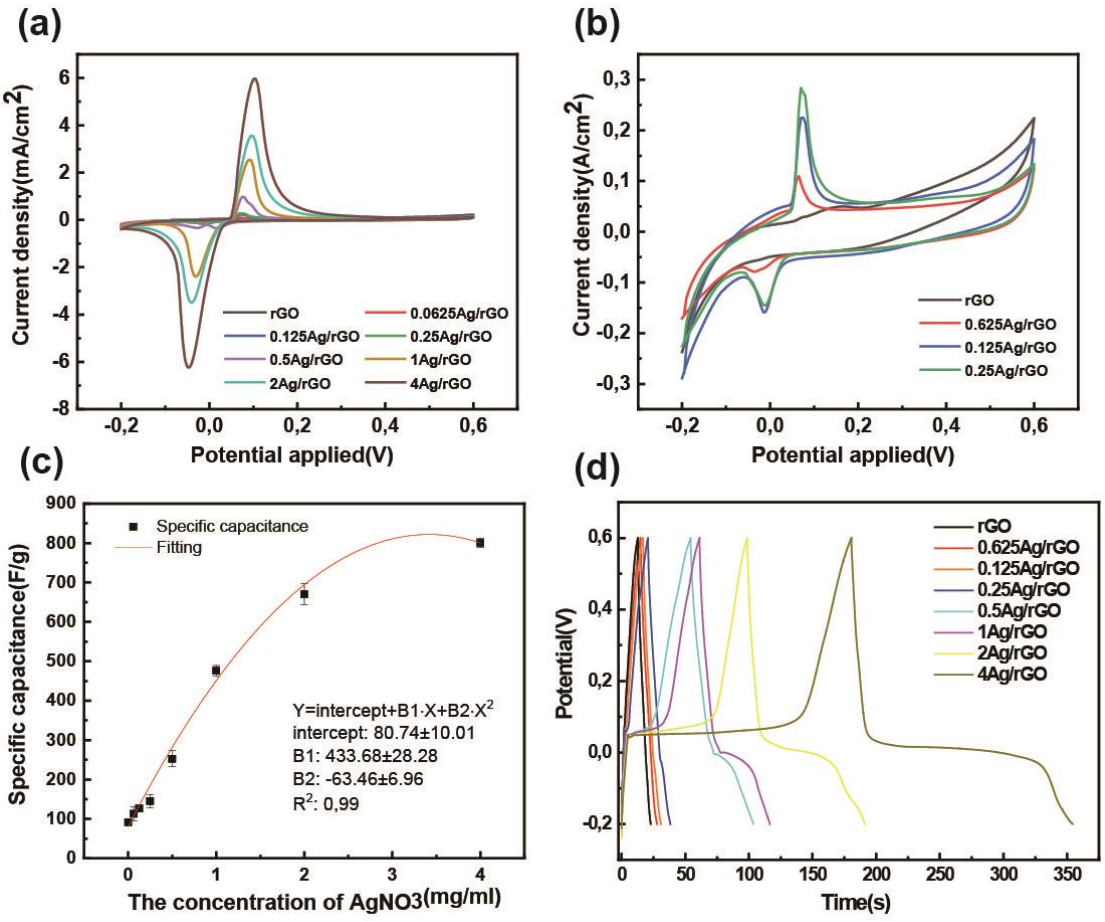

Figure 19. The CV responses of (a) various electrodes at 10 mV/s scan rate and (b) clear magnified CV curves from rGO to 0.25Ag/rGO, (c) the specific capacitance of electrodes with different $AgNO_3$ concentration, (d) GCD curves of different electrodes at 0.25 mA/cm^2.

Fig. 20a illustrates the current response of the 4Ag/rGO composite electrode at varying scan rates. It is observed that with an increase in scan rate, the peak current proportionally rises. The

oxidation peaks shift progressively to more positive values, whereas the reduction peaks are displaced in the reverse direction. This shift could be due to the internal resistance within the electrode [40]. Additionally, even at a high scan rate of 50 mV/s, distinct redox peaks are preserved, indicating that the constructed 4Ag/rGO electrode demonstrates excellent reversibility and fast charge transfer capabilities. **Fig. 20b** shows the specific capacitance of the 4Ag/rGO composite electrode across different scan rates. A slight decrease in capacitance is noted as the scan rate increases, possibly resulting from inadequate ion diffusion at the electrode-electrolyte interface at elevated scan rates, affecting ideal capacitive performance. The mechanical durability of the electrode was examined, as depicted in **Fig. 20c**. The findings reveal that the electrochemical attributes, such as peak current, are largely stable even after numerous bending tests, indicating robust mechanical flexibility and consistent electrochemical properties of the 4Ag/rGO composite electrode.

Moreover, electrochemical impedance spectroscopy (EIS) was utilized to evaluate the charging dynamics and capacitive properties. **Fig. 20d** presents the Nyquist plot for the fabricated electrodes. The inset in **Fig. 20d** details the equivalent circuit components, with Rs indicating the ohmic resistance of the solution between the working and reference electrodes, R_{ct} denoting the charge transfer resistance at the electrode-solution interface, CPE representing the constant phase element at this interface, and $W_0$the Warburg impedance. Analysis from the Nyquist plot reveals that the Rs for the 4Ag/rGO electrode (4.94 Ω) is considerably lower than that for the rGO (10.47 Ω). It is also notable that the slope at low frequencies in the Nyquist plot can be utilized to evaluate capacitive behaviour. In an ideal supercapacitor, the EIS plot would display a line perpendicular to the real axis [41]. Comparisons indicate that the Nyquist plot of the 4Ag/rGO more closely approximates this ideal state, suggesting enhanced capacitive performance

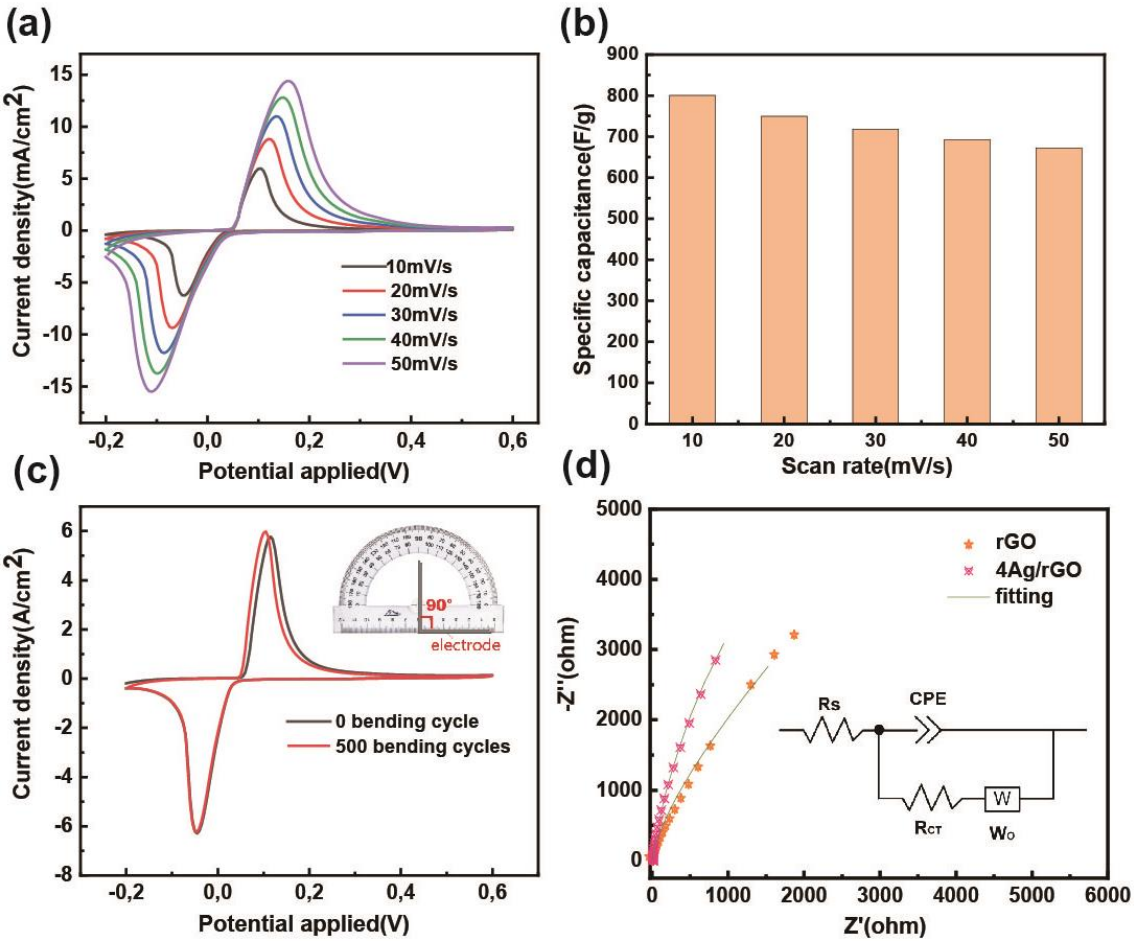

Figure 20. (a) The CV curves of 4Ag/rGO electrodes at various scan rates and (b) the specific capacitance of different 4Ag/rGO electrodes calculated at different scan rates, (c) CV curves of 4Ag/rGO under flat state and after being bent 500 times under 90°, at a scan rate of 10 mV/ s, (d) Nyquist plot of the 4Ag/rGO recorded in the frequency range of 0.01 Hz ~ 100 kHz.

From **Fig. 21a**, it is evident that the electrode has a prolonged discharge time at lower current densities, which becomes shorter as the current density rises. This reduction may be due to the restricted rate of ion transport and charge reorganization within the electrode at increased current densities, resulting in diminished capacitive performance. The durability over numerous cycles is crucial for the electrode materials used in supercapacitors. As indicated in **Fig. 21b**, over 2000 cycles, the specific capacitance of the rGO electrode slightly declined, but the capacitance retention of the 4Ag/rGO electrode improved from 100% to 104.9%, showcasing robust cycle stability. This high retention of capacitance is linked to the continuous activation and saturation of the 4Ag/rGO electrode by the electrolyte throughout extended charge-discharge cycles. Improved electrolyte penetration enhances access to the micro and mesopores of the electrodes, thus boosting charge retention through cycling [42]. Such exceptionally high capacitance retention rates exceeding 100% have also been reported in earlier research on porous carbon electrodes [43, 44]. Furthermore, a comparison of the discharge curves from the last three cycles to the first three cycles (illustrated in **Fig. 21c** and **21d**) reveals no notable degradation in performance, confirming the outstanding cyclic stability of the 4Ag/rGO electrode.

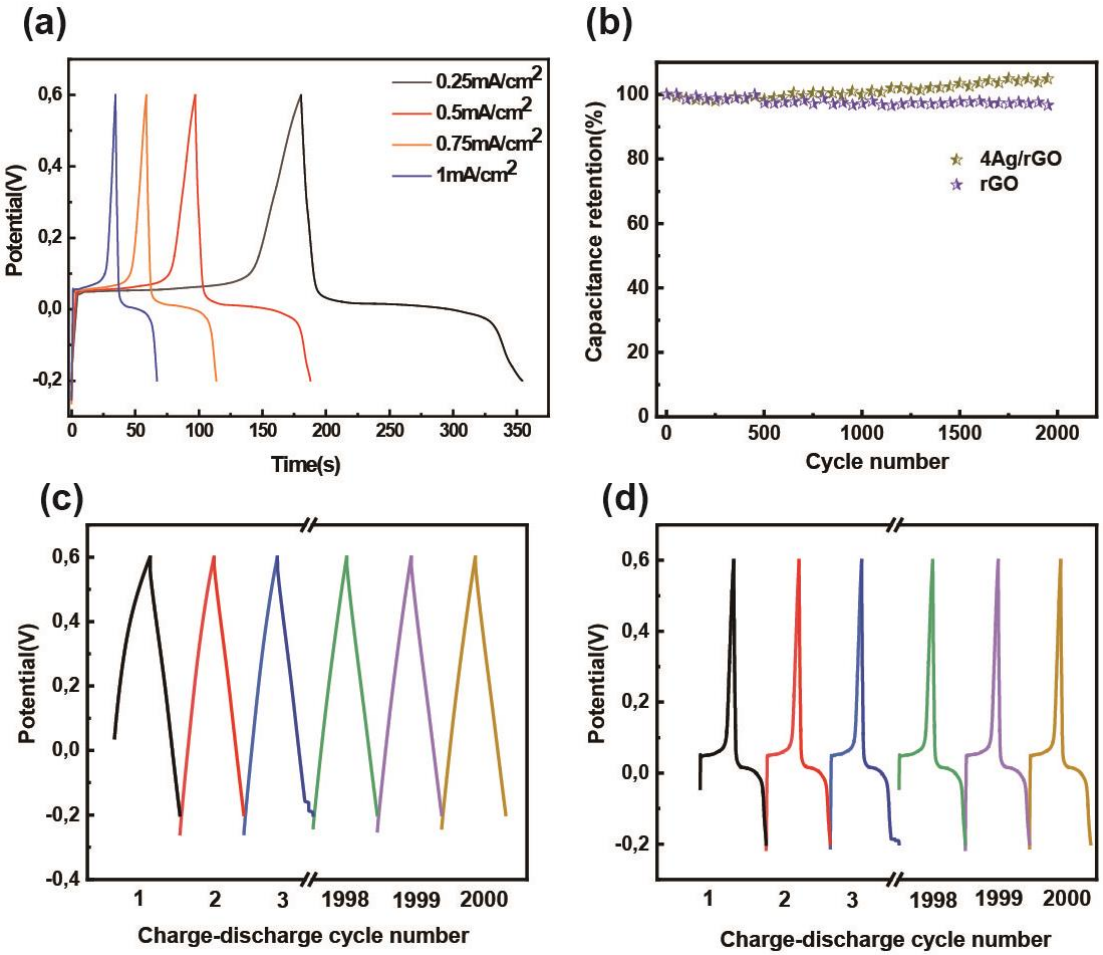

Figure 21. (a) GCD curves of 4Ag/rGO electrode at various current densities, and (b) cycle performance of the 4Ag/rGO electrode measured at a current density of 0.25 mA/cm^2. (c) the first three and the last three GCD cyclic curves of the rGO and (d) 4Ag/rGO electrode.

The Ragone plot is used to evaluate the 4Ag/rGO as electrode materials in **Fig.22**, alongside previously published research (seen in **Table 7**). Notably, the 4Ag/rGO composite electrode outshines other Ag-based carbonic materials, achieving an energy density of up to 70.9 Wh/kg and a power density of 1.41 kW/kg at a current density of 0.25 mA/cm^2. Even at a higher current density of 1 mA/cm^2, it sustains an energy density of 51.02 Wh/kg and a power density of 5.63 kW/kg. Typically, the energy density range for commercial supercapacitors lies between 5 and 30 Wh/kg. The supercapacitors we have developed with 4Ag/rGO offer an energy density that surpasses that of commercial options by more than double, enhancing their capacity to store more energy per unit weight. This substantial boost in energy density is crucial for fulfilling the requirements for lighter, more compact, and integrated solutions in microelectronic devices.

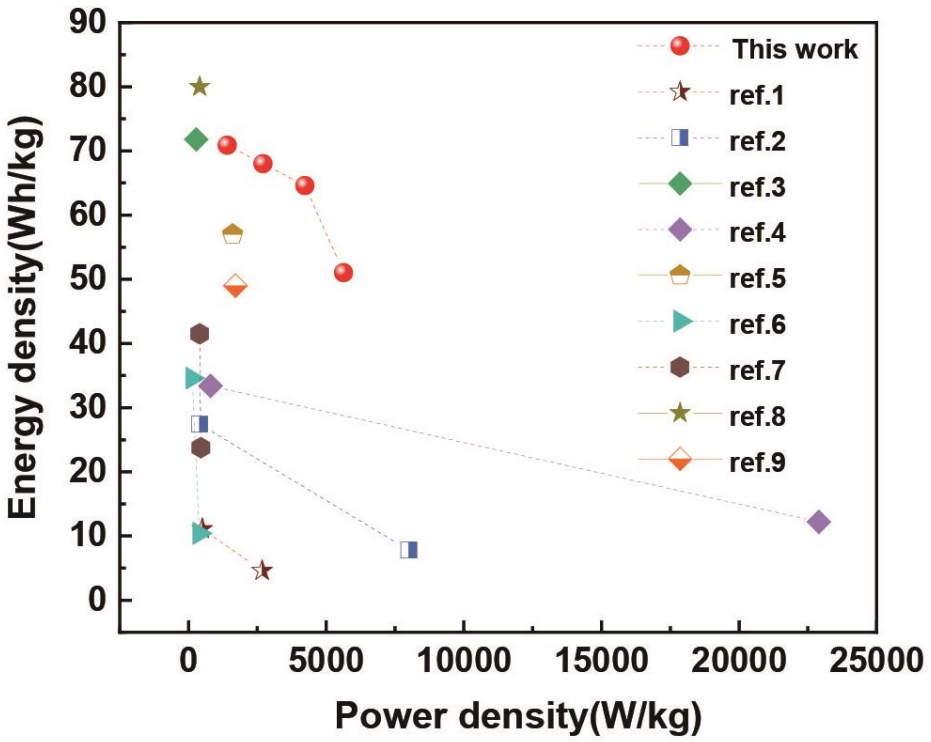

Figure 22. Ragone plot of the 4Ag/rGO electrode for the energy density and power density compared with reported literatures.

Table 7. The reported literatures shown in the Ragone plot

Number of references	Techniques and materials	reference
ref.1	Seed-mediated growing Ag@rGO hybrid electrode	[45]
ref.2	Chemical co-precipitated Mn_3O_4/rGO	[46]
ref.3	Electrochemical deposited γ -MnO_2/Ag/rGO	[47]
ref.4	Sacrificial template method prepared NiS//active carbon	[48]
ref.5	Successive ionic layer adsorption and reaction (SILAR) prepared MnO_2/Ag/GO composite	[49]
ref.6	Electroless plated AgNPs/rGO/CF composite	[50]
ref.7	Laser-assisted (LA) rGO//Ag-PPy	[51]
ref.8	In situ co-precipitated $(Ag_{0.50}Ni_{0.50})_{90}RGO_{10}$	[52]
ref.9	One-pot prepared Ag/Ni/rGO	[53]

6 Conclusion and future work

6.1 In-situ reduced rGO printed PVDF all-solid-state supercapacitor

In this part, we applied an in-situ reduction technique, where rGO is embedded onto a PVDF membrane using inkjet printing technology to create lightweight, flexible, all-solid-state supercapacitors. As the number of printing passes increased, there was a consistent reduction in the surface resistance of the printed rGO layers, which stabilized after five passes. EDX, FTIR/Raman, and XPS analyses confirmed that in-situ reduction by AA effectively decreased the oxygenated functional groups in GO. This recovery of electrical conductivity in rGO establishes a robust basis for its future electrochemical performance. Electrochemical analysis using CV curves showed that the 1rGO/PVDF electrode exhibited the highest capacitance of 85.66 F/g at a scan rate of 10 mV/s, outperforming the 3rGO/PVDF and 5rGO/PVDF under identical conditions and demonstrated excellent flexibility. The 1rGO/PVDF electrode also showed a specific capacitance of 83.29 F/g at a current density of 2 A/g, according to GCD analysis, with an energy density of 7.5 Wh/kg and a power density of 1.04 kW/kg, surpassing many previously reported values. Moreover, the rGO/PVDF electrode displayed robust cycle stability, maintaining 93% efficiency after 4000 charge-discharge cycles at a current density of 2 A/g, indicating its superior electrochemical stability.

6.2 In-situ reduced Ag/rGO printed PP flexible supercapacitor

In conclusion, to enhance electrochemical properties, GO and $AgNO_3$ ink were deposited and, in situ, reduced using a RIP system to create an electrochemically active layer. This Ag/rGO layer, applied on a textile substrate, serves as a flexible working electrode and achieves a peak-specific capacitance of 800.30 F/g in a three-electrode configuration. It shows remarkable cycling stability, with its capacitance remaining intact after over 2000 charge/discharge cycles at a current density of 0.25 mA/cm^2. The composite electrode retains its electrochemical capabilities even after being bent and reaches a maximum energy density of 70.9 Wh/kg at a power density of 1.41 kW/kg, greatly exceeding many existing reports of graphene-based flexible supercapacitors. The superior capacitance performance and straightforward production process render the textile-based Ag/rGO composite electrode a compelling choice for the design and creation of high-energy density flexible energy storage solutions.

6.3 Future work

Through our research on rGO/PVDF all-solid-state supercapacitors and Ag/rGO printed PP flexible supercapacitors, we observed significant improvements in electrochemical performance following the incorporation of metallic AgNPs. However, to more comprehensively assess the practical application performance of supercapacitors, the following tests are necessary:

1. Long-term energy storage efficiency: conducting long-term discharge experiments is crucial to evaluate how long supercapacitors can maintain the operation of devices after being fully charged. This test is vital for assessing their endurance in real-world applications.
2. Integrated application performance testing: using supercapacitors to power LED lights or other small electronic devices after charging will help verify their utility in practical applications.
3. Continuous use and reuse testing: subjecting supercapacitors to multiple charge-discharge cycles is essential to simulate their performance variability and reliability over prolonged usage.

7 References

[1] R. Kumar, S.M. Youssry, K.Z. Ya, W.K. Tan, G. Kawamura, A.J.D. Matsuda, R. Materials, Microwave-assisted synthesis of Mn3O4-Fe2O3/Fe3O4@ rGO ternary hybrids and electrochemical performance for supercapacitor electrode, 101 (2020) 107622.

[2] I.S. El-Hallag, M.N. El-Nahass, S.M. Youssry, R. Kumar, M.M. Abdel-Galeil, A.J.E.A. Matsuda, Facile in-situ simultaneous electrochemical reduction and deposition of reduced graphene oxide embedded palladium nanoparticles as high performance electrode materials for supercapacitor with excellent rate capability, 314 (2019) 124-134.

[3] T. Juntunen, H. Jussila, M. Ruoho, S. Liu, G. Hu, T. Albrow‐Owen, L.W. Ng, R.C. Howe, T. Hasan, Z.J.A.F.M. Sun, Inkjet printed large‐area flexible few‐layer graphene thermoelectrics, 28(22) (2018) 1800480.

[4] J. Khan, M.J.F. Mariatti, P. Electronics, In-situ graphene oxide reduction via inkjet printing using natural reducing inks, 8(3) (2023) 035009.

[5] S. Lv, S. Ye, C. Chen, Y. Zhang, Y. Wu, Y. Wang, R. Tang, M. De Souza, X. Liu, X.J.J.o.M.C.C. Zhao, Reactive inkjet printing of graphene based flexible circuits and radio frequency antennas, 9(38) (2021) 13182-13192.

[6] J. Kastner, T. Faury, H.M. Außerhuber, T. Obermüller, H. Leichtfried, M.J. Haslinger, E. Liftinger, J. Innerlohinger, I. Gnatiuk, D.J.M.e. Holzinger, Silver-based reactive ink for inkjet-printing of conductive lines on textiles, 176 (2017) 84-88.

[7] Y. Yang, V.J.D. Naarani, pigments, Improvement of the lightfastness of reactive inkjet printed cotton, 74(1) (2007) 154-160.

[8] T. Reinheimer, R. Azmi, J.R.J.A.a.m. Binder, interfaces, Polymerizable ceramic ink system for thin inkjet-printed dielectric layers, 12(2) (2019) 2974-2982.

[9] Q. Ke, J.J.J.o.M. Wang, Graphene-based materials for supercapacitor electrodes–A review, 2(1) (2016) 37-54.

[10] J. Hu, Z. Kang, F. Li, X.J.C. Huang, Graphene with three-dimensional architecture for high performance supercapacitor, 67 (2014) 221-229.

[11] N. Bardi, T. Giannakopoulou, A. Vavouliotis, C.J.A.A.N.M. Trapalis, Electrodeposited films of graphene, carbon nanotubes, and their mixtures for supercapacitor applications, 3(10) (2020) 10003-10013.

[12] J.-S. Lee, S.-I. Kim, J.-C. Yoon, J.-H.J.A.n. Jang, Chemical vapor deposition of mesoporous graphene nanoballs for supercapacitor, 7(7) (2013) 6047-6055.

[13] C. Zhu, X. Dong, X. Mei, M. Gao, K. Wang, D.J.J.o.M.S. Zhao, Direct laser writing of MnO2 decorated graphene as flexible supercapacitor electrodes, 55(36) (2020) 17108-17119.

[14] Z. Stempien, M. Khalid, M. Kozicki, M. Kozanecki, H. Varela, P. Filipczak, R. Pawlak, E. Korzeniewska, E.J.S.M. Sąsiadek, In-situ deposition of reduced graphene oxide layers on textile surfaces by the reactive inkjet printing technique and their use in supercapacitor applications, 256 (2019) 116144.

[15] I. Miccoli, F. Edler, H. Pfnür, C.J.J.o.P.C.M. Tegenkamp, The 100th anniversary of the four-point probe technique: the role of probe geometries in isotropic and anisotropic systems, 27(22) (2015) 223201.

[16] F. Azadian, O. Asif, A.C.J.E.T. Rastogi, Flexible, Thin-Layer Solid-State Supercapacitor Based on V2O5-Graphene Composite Electrode and Ionic Liquid Gel Polymer Electrolyte for Portable Electronic Systems, 97(7) (2020) 35.

[17] J. Huang, S. Peng, J. Gu, G. Chen, J. Gao, J. Zhang, L. Hou, X. Yang, X. Jiang, L.J.M.H. Guan, Self-powered integrated system of a strain sensor and flexible all-solid-state supercapacitor by using a high performance ionic organohydrogel, 7(8) (2020) 2085-2096.

[18] Y.-C. Chen, Y.-K. Hsu, Y.-G. Lin, Y.-K. Lin, Y.-Y. Horng, L.-C. Chen, K.-H.J.E.A. Chen, Highly flexible supercapacitors with manganese oxide nanosheet/carbon cloth electrode, 56(20) (2011) 7124-7130.

[19] Z. Niu, Y. Zhang, Y. Zhang, X. Lu, J.J.J.o.A. Liu, Compounds, Enhanced electrochemical performance of three-dimensional graphene/carbon nanotube composite for supercapacitor application, 820 (2020) 153114.

[20] B. Ding, D. Guo, Y. Wang, X. Wu, Z.J.J.o.P.S. Fan, Functionalized graphene nanosheets decorated on carbon nanotubes networks for high performance supercapacitors, 398 (2018) 113-119.

[21] S. Xu, X. Liang, K. Ge, H. Yuan, G.J.A.A.E.M. Liu, Supramolecular Gel Electrolyte-Based Supercapacitors with a Comparable Dependence of Electrochemical Performances on Electrode Thickness to Those Based on Bulk Electrolyte Solutions, 5(3) (2022) 2929-2936.

[22] X. Li, J. Shao, S.-K. Kim, C. Yao, J. Wang, Y.-R. Miao, Q. Zheng, P. Sun, R. Zhang, P.V.J.N.c. Braun, High energy flexible supercapacitors formed via bottom-up infilling of gel electrolytes into thick porous electrodes, 9(1) (2018) 2578.
[23] G.K. Veerasubramani, K. Krishnamoorthy, S. Radhakrishnan, N.-J. Kim, S.J.J.I.j.o.h.e. Kim, Synthesis, characterization, and electrochemical properties of CoMoO4 nanostructures, 39(10) (2014) 5186-5193.
[24] B.G. Choi, J. Hong, W.H. Hong, P.T. Hammond, H.J.A.n. Park, Facilitated ion transport in all-solid-state flexible supercapacitors, 5(9) (2011) 7205-7213.
[25] L. Yuan, X.-H. Lu, X. Xiao, T. Zhai, J. Dai, F. Zhang, B. Hu, X. Wang, L. Gong, J.J.A.n. Chen, Flexible solid-state supercapacitors based on carbon nanoparticles/MnO2 nanorods hybrid structure, 6(1) (2012) 656-661.
[26] Y. Liu, J. Zhou, L. Chen, P. Zhang, W. Fu, H. Zhao, Y. Ma, X. Pan, Z. Zhang, W.J.A.a.m. Han, interfaces, Highly flexible freestanding porous carbon nanofibers for electrodes materials of high-performance all-carbon supercapacitors, 7(42) (2015) 23515-23520.
[27] C.H. Kim, B.-H.J.E.A. Kim, Effects of thermal treatment on the structural and capacitive properties of polyphenylsilane-derived porous carbon nanofibers, 117 (2014) 26-33.
[28] T. Zheng, M.H. Tahmasebi, B. Li, Y. Li, S. Ran, T.S. Glen, K.H. Lam, I.S. Choi, S.T.J.C. Boles, Sputtered titanium nitride films on titanium foam substrates as electrodes for high‐power electrochemical capacitors, 5(16) (2018) 2199-2207.
[29] T. Le, Y. Yang, Z. Huang, F.J.J.o.P.S. Kang, Preparation of microporous carbon nanofibers from polyimide by using polyvinyl pyrrolidone as template and their capacitive performance, 278 (2015) 683-692.
[30] T. Chen, H. Peng, M. Durstock, L.J.S.r. Dai, High-performance transparent and stretchable all-solid supercapacitors based on highly aligned carbon nanotube sheets, 4(1) (2014) 3612.
[31] Y. Gao, Y. Zhou, W. Xiong, L. Jiang, M. Mahjouri-Samani, P. Thirugnanam, X. Huang, M. Wang, L. Jiang, Y.J.A.M. Lu, Transparent, flexible, and solid-state supercapacitors based on graphene electrodes, 1(1) (2013).
[32] P.-C. Chen, G. Shen, S. Sukcharoenchoke, C.J.A.P.L. Zhou, Flexible and transparent supercapacitor based on In2O3 nanowire/carbon nanotube heterogeneous films, 94(4) (2009).
[33] J. Broda, C. Slusarczyk, J. Fabia, A.J.T.r.j. Demsar, Formation and properties of polypropylene/stearic acid composite fibers, 86(1) (2016) 64-71.
[34] J.P.J.A.m. Vermeulen, processes, New developments in FESEM technology, 163(8) (2005) 33-37.
[35] L. Dong, Y. Ding, W. Huo, W. Zhang, J. Lu, L. Jin, Y. Zhao, G. Wu, Y.J.U.s. Zhang, A green and facile synthesis for rGO/Ag nanocomposites using one-step chemical co-reduction route at ambient temperature and combined first principles theoretical analyze, 53 (2019) 152-163.
[36] G. Liu, Y. Wang, X. Pu, Y. Jiang, L. Cheng, Z.J.A.S.S. Jiao, One-step synthesis of high conductivity silver nanoparticle-reduced graphene oxide composite films by electron beam irradiation, 349 (2015) 570-575.
[37] Y.C.G. Kwan, G.M. Ng, C.H.A.J.T.s.f. Huan, Identification of functional groups and determination of carboxyl formation temperature in graphene oxide using the XPS O 1s spectrum, 590 (2015) 40-48.
[38] P.K. Kalambate, R.A. Dar, S.P. Karna, A.K.J.J.o.P.S. Srivastava, High performance supercapacitor based on graphene-silver nanoparticles-polypyrrole nanocomposite coated on glassy carbon electrode, 276 (2015) 262-270.
[39] N.R. Chodankar, H.D. Pham, A.K. Nanjundan, J.F. Fernando, K. Jayaramulu, D. Golberg, Y.K. Han, D.P.J.S. Dubal, True meaning of pseudocapacitors and their performance metrics: asymmetric versus hybrid supercapacitors, 16(37) (2020) 2002806.
[40] S. Khamlich, T. Khamliche, M. Dhlamini, M. Khenfouch, B. Mothudi, M.J.J.o.c. Maaza, i. science, Rapid microwave-assisted growth of silver nanoparticles on 3D graphene networks for supercapacitor application, 493 (2017) 130-137.
[41] A. Jagadale, V. Kumbhar, D. Dhawale, C.J.E.A. Lokhande, Performance evaluation of symmetric supercapacitor based on cobalt hydroxide [Co (OH) 2] thin film electrodes, 98 (2013) 32-38.
[42] D. Gandla, X. Wu, F. Zhang, C. Wu, D.Q.J.A.o. Tan, High-performance and high-voltage supercapacitors based on N-doped mesoporous activated carbon derived from dragon fruit peels, 6(11) (2021) 7615-7625.
[43] M.D. Mehare, A.D. Deshmukh, S.J.J.o.M.S. Dhoble, Preparation of porous agro-waste-derived carbon from onion peel for supercapacitor application, 55(10) (2020) 4213-4224.
[44] C. Ding, T. Liu, X. Yan, L. Huang, S. Ryu, J. Lan, Y. Yu, W.-H. Zhong, X.J.N.-M.L. Yang, An ultra-microporous carbon material boosting integrated capacitance for cellulose-based supercapacitors, 12 (2020) 1-17.

[45] W. Tuichai, A. Karaphun, C.J.J.o.A. Ruttanapun, Compounds, Ag nanomaterials deposited reduced graphene oxide nanocomposite as an advanced hybrid electrode material for asymmetric supercapacitor device, 849 (2020) 156516.
[46] Y. Zhou, L. Guo, W. Shi, X. Zou, B. Xiang, S.J.M. Xing, Rapid production of Mn3O4/rGO as an efficient electrode material for supercapacitor by flame plasma, 11(6) (2018) 881.
[47] S. Sun, Y. Liu, G. Jiang, B. Yu, U. Evariste, P.J.E.M.L. Ma, Electrochemical Deposition of γ-MnO 2 on Ag/rGO Hybrid Films as Flexible Electrode Materials for Asymmetric Supercapacitor, 15 (2019) 331-341.
[48] J. Zhao, B. Guan, B. Hu, Z. Xu, D. Wang, H.J.E.A. Zhang, Vulcanizing time controlled synthesis of NiS microflowers and its application in asymmetric supercapacitors, 230 (2017) 428-437.
[49] V. Mane, S. Kale, S. Ubale, V. Lokhande, C.J.M.T.C. Lokhande, Enhanced specific energy of silver-doped MnO2/graphene oxide electrodes as facile fabrication symmetric supercapacitor device, 20 (2021) 100473.
[50] Z. Karami, M. Youssefi, K. Raeissi, M.J.E.A. Zhiani, An efficient textile-based electrode utilizing silver nanoparticles/reduced graphene oxide/cotton fabric composite for high-performance wearable supercapacitors, 368 (2021) 137647.
[51] S.A. Hashemi, H.R. Naderi, S.M. Mousavi, S. Bahrani, M. Arjmand, A.M. Dimiev, S.J.C. Ramakrishna, Synergic effect of laser-assisted graphene with silver nanowire reinforced polyindole/polypyrrole toward superior energy density, 188 (2022) 276-288.
[52] M. Chandel, P. Makkar, N.N.J.A.A.E.M. Ghosh, Ag–Ni nanoparticle anchored reduced graphene oxide nanocomposite as advanced electrode material for supercapacitor application, 1(7) (2019) 1215-1224.
[53] P. Makkar, N.N.J.I. Ghosh, E.C. Research, High-performance all-solid-state flexible asymmetric supercapacitor device based on a Ag–Ni nanoparticle-decorated reduced graphene oxide nanocomposite as an advanced cathode material, 60(4) (2021) 1666-1674.

8 List of publications by the author

8.1 Publications in journals

1. Peng Q, Tan X, Venkataraman M, et al. Tailored expanded graphite based PVDF porous composites for potential electrostatic dissipation applications[J]. *Diamond and Related Materials*, 2022, 125: 108972. https://doi.org/10.1016/j.diamond.2022.108972 (Scopus, Q2, IF: 3.806)

2. Peng Q, Tan X, Venkataraman M, et al. Effects of ultrasonic-assisted nickel pretreatment method on electroless copper plating over graphene[J]. *Scientific Reports*, 2022, 12(1): 21159. https://doi.org/10.1038/s41598-022-25457-y (Scopus, Q1, IF: 4.996)

3. Peng Q, Tan X, Xiong X, et al. Insights into the large-size graphene improvement effect of the mechanical properties on the epoxy/glass fabric composites[J]. *Polymer Composites*, 2023, 44(11): 7430-7443. https://doi.org/10.1002/pc.27635 (Scopus, Q1, IF: 5.2)

4. Peng Q, Yang K, Venkataraman M, et al. Preparation of electrosprayed composite coated microporous filter for particulate matter capture[J]. *Nano Select*, 2022, 3(3): 555-566. https://doi.org/10.1002/nano.202100186 (Scopus)

5. Peng, Q., et al. In situ reduction of nanofabric-based graphene flexible all-solid-state supercapacitor via inkjet printing system. (under 1st round review by *Journal of Energy Storage*) (Scopus, Q1, IF: 9.4)

6. Peng, Q., et al. One step eco-friendly in-situ reduction of graphene oxide/silver nanoparticle layer via reactive inkjet printing for flexible high-performance supercapacitor (under 1st round review by *Nano Materials Science*) (Scopus, Q1, IF: 8.2)

7. Tan X, Peng Q, Yang K, et al. Preparation and Characterization of corn husk nanocellulose coating on electrospun polyamide 6[J]. *Alexandria Engineering Journal*, 2022, 61(6): 4529-4540. https://doi.org/10.1016/j.aej.2021.10.011 (Scopus, Q1, IF: 6.628)

8. Tan X, Peng Q, Subrova T, et al. Characterization of Cellulose/Polyvinyl Alcohol/Expanded Graphite 3D Porous Foam and Adsorption of Methylene Blue[J]. *Journal of Natural fibers*, 2023, 20(1): 2190189. https://doi.org/10.1080/15440478.2023.2190189 (Scopus, Q1, IF: 3.507)

9. Yang K, Peng Q, Venkataraman M, et al. Hydrophobicity, water moisture transfer and breathability of PTFE-coated viscose fabrics prepared by electrospraying technology and sintering process[J]. *Progress in Organic Coatings*, 2022, 165: 106775. https://doi.org/10.1016/j.porgcoat.2022.106775 (Scopus, Q1, IF: 6.206)

10. Tan X, Jiang Y, Peng Q, et al. Development and characterization of silane crosslinked cellulose/graphene oxide conductive hydrophobic membrane[J]. *Cellulose*, 2023, 30(7): 4561-4574. https://doi.org/10.1007/s10570-023-05079-x (Scopus, Q1, IF: 6.123)

11. Tan, X, Jiang, Y, Puchalski, M, Peng, Q, Hu, S, et al. The multifunctional flexible conductive viscose fabric prepared by thiol modification followed by copper plating[J]. *Cellulose*, 2024: 1-16. 10.1007/s10570-024-05764-5 (Scopus, Q1, IF: 6.123)

8.2 Contribution in conference proceeding

1. Q. Peng, S. Xiao, X. Tan, K. Yang, Y. Wang, T. Yang, D. Wang, S. Hu, X. Xiong, M. Venkataraman, J. Militký, Dendrimer-grafted PLGA nanofibrous matrix-mediated gene delivery systems, Textile Bioengineering and Informatics Symposium Proceedings 2020 - 13th Textile Bioengineering and Informatics Symposium, TBIS 2020, 2020, pp. 152-158.

3. Q. Peng, X. Tan, M. Venkataraman, J. Militký, Expanded Graphite/PVDF Porous film for Electrostatic Dissipation. CLOTECH 2022 Sep.5-8th.

4. Q. Peng, X. Tan, M. Venkataraman, at el. Nickel pretreatment under ultrasound for electroless copper plating on graphene. STRUTEX 2022.

5. Peng Q, Venkatarman M, et al. STUDY ON G5.NH2-MODIFIED PLGA ELECTROSPINNING SUBSTRATE AS GENE DELIVERY SYSTEM. AUTEX 2021-20th.

6. K. Yang, Q. Peng, M. Venkataraman, J. Novotna, X. Xiong, J. Wiener, Y. Wang, X. Tan, G. Zhu, J. Yao, J. Militký, Hydrophobic Breathable Fabric via Electrospraying Technology. Autex Conference 2021.

7. Y. Wang, M. Venkataraman, K. Yang, Q. Peng, S. Hu, J. Militký. DEVELOPMENT OF PDMS/COPPER-COATED GRAPHITE ELEASTOMER FOR STRAIN SENSOES APPLICATION. CLOTECH 2022 Sep.5-8th.

8. X. Tan, Q. Peng, et al. Preparation of cellulose-based foam composites and their application in dye adsorption. TBIS 2022 Sep.8th.

9. K. Shah, Q. Peng, M. Venkataraman, J. Militký. Battery Performances and Thermal Stability of Polypropylene Nonwoven Separator for Li-ion Battery. NIA 2022.

8.3 Citations

1. Peng Q, Tan X, Venkataraman M, et al. Tailored expanded graphite based PVDF porous composites for potential electrostatic dissipation applications[J]. *Diamond and Related Materials*, 2022, 125: 108972. https://doi.org/10.1016/j.diamond.2022.108972

(*Citations*:5)

2. Peng Q, Tan X, Venkataraman M, et al. Effects of ultrasonic-assisted nickel pretreatment method on electroless copper plating over graphene[J]. *Scientific Reports*, 2022, 12(1): 21159. https://doi.org/10.1038/s41598-022-25457-y

(*Citations*:2)

4. Peng Q, Tan X, Xiong X, et al. Insights into the large-size graphene improvement effect of the mechanical properties on the epoxy/glass fabric composites[J]. *Polymer Composites*, 2023, 44(11): 7430-7443. https://doi.org/10.1002/pc.27635

(*Citations*:1)

5. Peng Q, Yang K, Venkataraman M, et al. Preparation of electrosprayed composite coated microporous filter for particulate matter capture[J]. *Nano Select*, 2022, 3(3): 555-566. https://doi.org/10.1002/nano.202100186

(*Citations*:7)

Curriculum Vitae

Name: Qingyan Peng

Tel: +420 704913498

E-mail: qingyan.peng@tul.cz

Institution: Department of Material Engineering, Faculty of Textile Engineering, Technical University of Liberec, 461 17 Liberec, Czech Republic

Address: 17 Listopadu, 584/2, 46015, Liberec, Czech Republic.

Nationality: China

Education

Ph.D. | Jan.2020 - Now | Technical University of Liberec, Czech Republic
Major: Textile engineering
Dissertation topic： New system of electrodes for supercapacitor
Research area: Focuses on reduced graphene oxide composite films on textile materials for applications in supercapacitors and electromagnetic interference shielding. It also involves the fabrication and mechanical property evaluation of graphene-based resin reinforced materials. Additionally, explores electrostatic sprayed coatings of expanded graphite/PTFE for particle capture, and the preparation of metal-carbon composite nanoparticles by chemical plating.
Research tools: Scanning electron microscope (SEM), Fourier transform infrared spectroscopy (FTIR), x-ray photoelectron spectroscopy (XPS), energy dispersive X-ray spectroscopy (EDX), electrical conductivity tester, x-ray diffraction (XRD), Raman spectroscopy, differential scanning calorimetry (DSC), thermogravimetric analysis (TGA), and Instron.

Master degree | Sep. 2015 – Jun. 2018 | Wuhan Textile University, China
Major: Textile engineering
Dissertation topic： Study of G5.NH_2-grafted electrospun PLGA nanofibers substrate-mediated gene delivery systems.
Research area: Preparation and characterization of PAMAM dendrimer-grafted PLGA nanofibers for gene delivery; Build the drug loaded nano-system based on poly (L-lactic acid) (PLLA) for tissue engineering.
Research tools: Scanning electron microscope (SEM), Fourier transform infrared spectroscopy (FTIR), x-ray photoelectron spectroscopy (XPS), antibacterial test, gene delivery test kit, electrospinning machine.

Bachelor degree | Sep. 2011- Jun. 2015 | Wuhan Textile University, China
Major: Textile engineering
Dissertation topic：Water-repellent treatment of cotton fabric
Main subjects: Textile materials, Textile physical, C++, Chemical, Retail, etc.
Research tools: Water contact angle tester, Instron, Scanning electron microscope (SEM), thickness gauge

Internship

- July. 2015-Aug. 2015

Jihua 3542 Textile Co., Ltd., China

studying the manufacturing processes of linen-blended and slubbed linen-like fabrics, fine-denier high-count functional fabrics, and various camouflage canvas fabrics.

- Feb. 2022-May. 2022

Wood K plus –Competence Center for Wood Composites and Wood Chemistry, Austria.

The fabrication of copper deposited graphene with a novel and facile pretreatment method through electroless plating.

- Sep. 2022-Dec. 2022

Lodz University of Technology, Institute of Textile Architecture, Poland.

Learned the operation methods of the inkjet printing system and the usage procedures and methods of the electrochemical workstation.

- Sep. 2023-Dec. 2023

Lodz University of Technology, Institute of Textile Architecture, Poland.

Learned the operation methods of FTIR equipment.

Reccomendation of the supervisor

01.11.2024

Liberec

Recommendation for the PhD defence of Ms. Qingyan Peng

Ms. Qingyan Peng started her PhD in 2020 under my supervision. Her PhD thesis titled "New System of Electrodes for Supercapacitor,, proposes a novel approach for developing flexible supercapacitors, which employs reactive inkjet printing (RIP) technology to deposit and in-situ reduce single/composite graphene inks on various fabric substrates. Utilizing advanced inkjet printing techniques, this method allows for precise material deposition and compositional tuning, enabling the fabrication of high-performance flexible electrodes suitable for supercapacitors. The superior capacitance performance and straightforward production process render the textile-based Ag/rGO composite electrode a compelling choice for the design and creation of high-energy density flexible energy storage solutions.

During her PhD, Ms. Peng confirmed her ability to perform high-quality research, which is already evident in her research outputs. She is a well-motivated, hard-working, and independent researcher. She is very knowledgeable in her topic of research and applies her intelligence to push the envelope of her research. Her disciplined approach towards research has enabled her to publish articles in high-impact peer-reviewed journals and international conferences. She has authored 11 impact factor journals, 9 international conferences and 2 book chapters. She has excellent potential, demonstrated by the high h-index of 5 for an early-stage researcher.

Ms. Peng has completed the coursework, the internship tenure of 6 months, the exam related to the internships, and the state exam, which is required for defending the thesis. She submitted her thesis in July 2024 and is defending her thesis in the given time frame. Based on the evaluation, the text content, figures, and tables of the dissertation work have been cited with references in accordance with the established rules.

I consider the thesis titled "New System of Electrodes for Supercapacitor,, to have excellent scientific relevance and potential and I highly recommend Ms. Qingyan Peng's thesis be accepted for defence.

Mohanapriya Venkataraman, M.Tech., M.F.Tech., Ph.D.
Supervisor
Department of Material Engineering
Faculty of Textile Engineering
Technical University of Liberec
Czech Republic

Opponent's reviews

Review to dissertation titled "New system of electrodes for supercapacitor"

Supercapacitor typically offer high power density but lower energy density, and the electrodes of supercapacitor are significantly influencing the energy density of supercapacitor. Therefore, how to improve the energy density of supercapacitor or how to develop a more suitable electrode has become a very important research topic.

This dissertation aims to develop a novel system of electrodes for flexible supercapacitors with high performance for energy storage. For this purpose, the Ph.D. candidate deposited reduced graphene oxide (rGO) on polyvinylidene fluoride (PVDF) nanofibrous membranes by inkjet printing, and also deposited Ag/rGO on polypropylene nonwovens by inkjet printing. By using this method, the rGO was deposited uniformly. In addition, the deposition of silver nanoparticles between rGO sheets prevented the aggregation of rGO, leading to an improvement of charge transfer rate and capacitive performance of the electrodes. Therefore, this dissertation work is innovative and solved some key issues of electrodes while using graphene and its derivatives.

In the section of State of the Art, the literature review covers the information of structure, classification, properties of graphene and its derivatives, fabrication of graphene and graphene derivatives composites, classification of supercapacitors, electrode materials for supercapacitors, synthesis approach for electrode materials, characterization techniques for supercapacitor properties, as well as current achievements and challenges in supercapacitor, which provide a comprehensive and detailed introduction of supercapacitor and electrode.

In the experimental section, the preparation of samples was described "electrode: firstly, depositing a gold layer with a thickness of around 20 - 50 nm onto the electrospun PVDF substrate as precursor current electrode. Subsequently, an electrode was constructed by depositing layers of rGO onto the existing current electrode's surface", "polymer electrolyte: Initially, 1g of H_2SO_4 was gradually introduced into 10 ml of distilled water. Sequentially, 1g of PVA was blended into the previously prepared H_2SO_4 solution at 80 ℃, accompanied by vigorous stirring until a clear solution was formed", "supercapacitor: a GF/F Whatman™ glass microfiber membrane separator was soaked in the PVA- H_2SO_4 polymer electrolyte. Finally, two rGO/PVDF freestanding electrodes were arranged in a sandwiched structure with the separator in between". The devices and processing parameters for preparing of electrode, polymer electrolyte and supercapacitor were also described clearly. The information of testing devices/equipment and procedures was given concisely. Therefore, the methodology was appropriate and the experiments were well-designed and implemented.

In the results and discussion section, the results of samples in terms of SEM, EDX, surface resistance, FTIR, Raman, XPS and Electrochemical characterizations were

clearly presented. Besides, the energy density and power density of samples for this dissertation work were compared with that of reported literatures, and the performance of samples from this dissertation work has advantages. The conclusions of this dissertation work are supported by the experimental results.

Generally speaking, this dissertation work was systematically designed and carried out, the dissertation was written logically and well-structured, the experiments and results were presented concisely, which provides significant contribution to electrodes and supercapacitor for energy storage.

During the Ph.D. study, the candidate has published 4 papers in journals with high impact factor, 2 papers under review, 4 international conference papers, and 2 book chapters, which indicates that the candidate has contributed a good research work to the dissertation area and got the recognition by peer review. Therefore, I recommend the Ph.D. dissertation for defence.

However, there are still some small questions,

1. The title "New Systeme of Electrodes for Superapacitor" could be "New System of Electrodes for Supercapacitor".
2. Section abstract in Chinese, the "AgNO3" could be "$AgNO_3$".
3. Page 30, "Because of its high theoretical strength, graphene, and its derivatives have been...", the comma after "graphene" can be deleted.
4. Page 50, table 4, why the units of concentration of GO dispersion are not the same, i.e. the unit can be either mg/mL or g/L.
5. Page 95, "the 1rGO/PVDF electrode exhibited the highest capacitance of 85.66 F/g at a scan rate of 10 mV/s", "The 1rGO/PVDF electrode also showed a specific capacitance of 83.29 F/g at a current density of 2 A/g", why the author use "highest capacitance" and "specific capacitance"? What are the differences?
6. The information of "requirements of electrode for supercapacitor" could be needed in the start of the art section. For instance, the range of electrical conductivity, porosity, pore size, specific surface area, thickness, mechanical strength thermal stability, etc.

Reviewer: 2024.08.26

Assoc. Prof. Guocheng Zhu

College of Textile Science and Engineering

(International institute of silk)

Zhejiang Sci-Tech University

THESIS ASSESSMENT REPORT

Date: October 12,2024

THESIS TITLE: New System of Electrodes for Supercapacitor

NAME OF CANDIDATE: Qingyan Peng

RECOMMENDATION:

This thesis is well written with systematic presentation of the research work carried out in the candidate's PhD study. The work is presented logically in the thesis to show the attempt to develop a novel approach for producing flexible supercapacitors, which employs reactive inkjet printing (RIP) technology to deposit and in-situ reduce single/composite graphene inks on various fabric substrates. This work is trying to use advanced inkjet printing techniques for precise material deposition and compositional tuning to fabricate high-performance flexible electrodes suitable for supercapacitors.

The candidate created ultralight pure reduced graphene oxide (rGO) all-solid-state supercapacitors with polyvinylidene difluoride (PVDF) electrospun nanofiber substrates, by using inkjet printing and optimized through in-situ chemical reduction with L-ascorbic acid (AA), which are analyzed using the Interface 1010E™ potentiostat to evaluate the impact of the rGO print layers on their electrochemical properties and other performance metrics.

Further, the candidate fabricated composite flexible supercapacitors with combining Ag nanoparticles (AgNPs) with rGO via RIP technology onto flexible polypropylene (PP) nonwoven fabrics by using a customized inkjet printing process with an additional print head to deposit silver nitrate (AgNO3) ink and GO ink and AA reducing agent simultaneously, followed by in-situ and synchronous reduction.

The morphology and structures of the rGO/PVDF electrodes and the Ag/rGO composite electrodes were characterized and their performances were evaluated in terms of electric surface resistance, specific capacitance, energy density and charge-discharge stability. Test data indicate that significant improvements in the performance criteria were achieved.

This study has made significant contribution to the development of advanced technologies for fabricating supper capacitor. The academic contribution of the study is important.

The candidate developed a methodological strategy to systematically address the objectives, as reported in the thesis.

- Chapter 1-Introduction: A general background has been provided.
- Chapter 2-Aim and objectives are provided.
- Chapter 3-Literature Review: Systematic review relevant work published with discussion and critical analysis of published related work and identify what has been developed in the relevant fields.
- Chapter 4-Experimental part: Described materials, equipment and super capacitor fabrication processes, as well as characterization and measurement methods.
- Chapter 5-Results and discussion: The results of morphology, structural and chemical features of fabricated materials on the "In-situ reduced rGO printed PVDF all-solid-

state supercapacitor" and the "In-situ reduced Ag/rGO printed PP flexible supercapacitor" are presented. The performances of the supercapacitors are presented systematically.

- Chapter 6: Conclusion and future work are presented.

The candidate has achieved the overall aim of the research. However, the documentation of this work needs to be improved to meet the requirements to represent an original contribution to the field of research, demonstrate an understanding of the entire body of work in the thesis, outline the relationship with existing literature and future developments and it must be a coherent body of related work. Specific comments are given below:

1. In Chapter 1, explain why this topic is important and how did you select this topic? Try to avoid using "we", as this thesis represents your own PhD research work.
2. In Chapter 2, how did you derive the aim and objectives? how are you sure that your research work is original? The logic relationships between the research gaps identified from the literature review and the objectives needs to be clarified.
3. In Chapter 2, explain what's logic of this thesis to represent an original contribution to the field of research, demonstrate an understanding of the entire body of work in the thesis, outline the relationship with existing literature and future developments and it must be a coherent body of related work. The logic framework of research gaps->objectives->methodology->thesis structure outline should be presented. (page 5)
4. In Chapter 2, the format of description of the objectives should be standardized. (Page 5)
5. In Chapter 3: What is the purpose of the literature review? Just learn and collect information? (Page 6)
6. In Chapter 3, lack of critical analysis in literature review, which are mainly descriptive. No research gaps have been identified. How is this literature review related to the objectives?
7. Lack of conclusion from the literature review. Elaborate what are the key findings of the literature reviews, what are the research gaps identified to justify the originality of your work.
8. In Chapter 4, clarify what are the research design/experimental design, as well as the data error treatment and relevant statistical methods applied.
9. In Chapter 5, what are the statistical significance between the results of with and without washing in Figure 21 page 65?
10. What are the data variations and statistical significance between the specific capacitance of different rGO/PVDF electrodes in Figure 28(d), page 76?
11. What is the statistical significance between the surface resistance of electrodes prepared with different concentrations of AgNO3 in Figure 35 (a)?
12. In Chapter 5, Add a summary of the key findings of the experimental work, not finish the Chapter without outline the key findings.
13. In Chapter 6, clarify what's the original contribution of this PhD work in the conclusion and its significance.

14. In Chapter 6, clarify whether the objectives of this PhD project set out in Chapter 2 have been achieved? and how?
15. In Chapter 6, clarify what's the limitation of this PhD research work?

I recommend that the candidate, Qingyan Peng, proceed to oral defense with revisions to address the above questions.

Yours sincerely

Prof. and Dr. Henry, Yi LI
Chair of Textile Science and Engineering
Department of Materials, The University of Manchester
Manchester M13 9PL, UK
Chairman, Textile Bioengineering and Informatics Society
Editor-in-Chief, Journal of Fiber Bioengineering and Informatics
Tel: +44 (0) 161 306 2676
Email: henry.yili@manchester.ac.uk